Materials Today Communications 42 (2025) 111416

Contents lists available at ScienceDirect

Materials Today Communications

journal homepage: www.elsevier.com/locate/mtcomm

Exploring the functional properties of *Plodia interpunctella* silk fibers as a natural biopolymer for biomaterial applications

Lauren E. Eccles, Elizabeth L. Aikman, Jasmine B. McTyer, Isabel L. Matías Cruz, Adelyn L. Richgels, Whitney L. Stoppel *

Department of Chemical Engineering, University of Florida, Gainesville, FL, USA

ARTICLE INFO

Keywords:
Natural biopolymers
Natural fibers
Silk fibroin
Crystallinity
Elastic modulus

ABSTRACT

Renewable and degradable materials, formed using biopolymers as material precursors, are sought after in pharmaceutical, biomedical, and industrial fields. Silk-based biomaterials, primarily derived from the silk fibroin protein of the *Bombyx mori* (*B. mori*) silkworm, have advantageous mechanical properties, biocompatibility, and commercial availability. Recent efforts aim to expand the range of achievable silk-based biomaterial properties via alternative sources of silk proteins with different sequences and structures. These structural distinctions drive differences in physical and chemical properties of silk fibers, primarily due to the varying degree of crystallinity in the polymers. For the development of alternative silk-based materials, silk from *Plodia interpunctella* (*P. interpunctella*), a small agricultural pest that infests and damages food products via silk production, is evaluated. Early investigations have highlighted differences between *P. interpunctella* and *B. mori* silk fibroin proteins, however *P. interpunctella* silk still largely lacks characterization and optimization on both the silk fiber and bulk material level. This work evaluates the structural, thermal, mechanical, and cell-material properties of non-degummed and degummed *P. interpunctella* silk as a raw material for biomaterial fabrication and discusses the benefits and limitations of these proteins as new biopolymers. Observed properties are used to identify links between silk fibroin protein sequence and fiber function in addition to forming hypotheses in how *P. interpunctella* silk-based biomaterials will perform in comparison to other natural biopolymers. Future work aims to develop methods to process *P. interpunctella* silk into material formats, utilizing the material characteristics determined here as a baseline for shifts in material performance.

1. Introduction

Natural biopolymers and fibers are investigated in biomaterial applications as an alternative to synthetic polymers to reduce production of environmental pollutants and use of non-renewable resources. Either produced directly by the native living organism or recombinantly produced to mimic the natural polymer, natural biopolymers and fibers (e.g., bamboo, cellulose, collagen, hemp, PLA, silk) have led to a variety of biomaterial and bio-composite applications across environmental, industrial, and human health fields because of their tunable mechanical strength, long-term stability, biocompatibility, degradability, and commercial availability [6,11,16–18]. Silks are a diverse class of natural protein fibers originating from a large distribution of silk-producing insects in the Lepidopteran and Araneae order [2,20,21]. Silk fibers vary across multiple structural levels and across species due to changing evolutionary needs such as housing, protective casings, and hunting [20] and environmental parameters such as temperature, humidity, and food sources [3,22–25]. Across most terrestrial insects, silk fibers are primarily composed of two parts, an inner fiber core and a fiber coating. The inner core is predominately composed of fibroins while the outer coating is formed from sericins and other proteins such as seroins or mucin-like proteins, where composition varies with each insect species and the purpose of the silk fiber. Fibroins are a class of proteins attributed to mechanical strength while the outer coating provides adhesive properties as well as other functions related to protecting the insect (e.g., defense against predators, antifungal or antibacterial properties). In the silk gland, these proteins self-assemble and fold to form a double stranded structure through silk spinning, a process driven by shear forces, shifts in pH and ionic strength, and changes in concentration [3,20,26–36].

Utilization of silk in material fabrication is a vast field, though it is largely dominated by the use of silk fibroin from the domesticated

* Correspondence to: 1006 Center Drive, PO Box 116005, Gainesville, FL 32611, USA.
E-mail address: Whitney.stoppel@ufl.edu (W.L. Stoppel).

https://doi.org/10.1016/j.mtcomm.2024.111416
Received 20 October 2024; Received in revised form 4 December 2024; Accepted 22 December 2024
Available online 24 December 2024

silkworm, *Bombyx mori* (*B. mori*), stemming from extensive cultivation for the textile industry [18,38]. *B. mori* silk fibroin is a structural protein composed of a heavy chain (~390 kDa) and light chain (~26 kDa) [17, 39], in which the former largely consists of amino acid repeats (GAGAGS) and is primarily responsible for the formation of β-sheet crystal structures, or β-solenoid structures, in silk [14,26]. The advantageous thermophysical properties of silk fibers are often attributed to crystalline units acting as crosslinks between silk proteins in the fiber [26]. These interacting crystalline units are also maintained in the end-biomaterial, giving rise to favorable capabilities such as inducible crystallinity to tune mechanical properties [18,40], degradation [41–43], and bioactive molecule stabilization [44,45]. However, the use of a singular source of raw material limits the variety of properties achievable in a material format (e.g., cell-material interactions, shear sensitivity) and the availability of the material source, prompting explorations into composite materials [6,46], chemical modification [47–51], and molecular engineering of silk proteins [18,19,49,52–54] to tailor properties for desired functions or improve scales of material production.

Another potential avenue to broaden the range of raw materials and achievable material properties for silk-based biomaterials lies in the biological diversity of silk-producing insects. Silk fibers produced by silkworms, spiders, and other species can differ largely in composition and structure, thermal and mechanical properties, and cytocompatibility [21,55,56] that bring about specific advantages in silk biomaterial formats or applications. For example, silk proteins from the *Antheraea mylitta* (*A. mylitta*) and *Antheraea pernyi* (*A. pernyi*) silkworms have an arginine glycine-aspartate (RGD) sequence that has been utilized to improve cell attachment and proliferation on silk films [57], porous sponges [58], and electrospun fibers [46]. Spider silk's reputational strength (*e.g.,* from *Euprosthenops australis, Araneus ventricosus*, or *Trichonephila clavipes*) has inspired new adhesives [59], elastomers, and artificial fibers for light transmission or water responsive contraction [59,60], with substantial advancements in sequences and spinning technologies over the last decade [52,61–64]. Caddisflies, aquatic silk-spinning insects, produce silk fibers with unique underwater adhesive properties capable of strength recovery post-strain [65]. While quite exciting, the application of caddisfly silk proteins across biomaterials and tissue engineering applications has yet to be realized. Utilization of these alternative silks is an existing and ever-expanding field in silk biomaterials as new silks are collected, characterized, and developed for future applications.

Plodia interpunctella (*P. interpunctella, Pi*), the pantry moth, is a small agricultural pest that has largely been studied to understand the growth and development of larva relevant in agricultural product damage. However, recent works have proposed *P. interpunctella* silk fibers for biomedical applications [23,66,67]. *P. interpunctella* silkworms can be reared in a laboratory setting with control over environmental parameters (temperature, humidity, diet), minimizing batch-to-batch variability in produced silk fibers and larval life cycles [23,24], which can be a common issue in silks reared outdoors where changes in climate impact the silk production and properties of the fibers [22,23,25]. During their life cycle, *P. interpunctella* larvae lay silk on the surfaces of their rearing container in scalable quantities in the 4th-5th instar phase, termed wandering silk [23,24,68]. This wandering silk accumulates in thin sheets that can be collected without interruption of insect pupation, enabling completion of the life cycle [23], highlighting the potential commercial applicability of these materials.

While investigations into the heavy fibroin protein sequence have compared *P. interpunctella* to other similar silk producing insects [69] and initial work has explored the proteins present in the *P. interpunctella* silk fiber for applications in human health [66,67], a comprehensive evaluation of silk fiber characteristics has not been presented. Given the known differences in amino acid sequences, this work aims to begin to connect the composition of the silk fiber, the sequence of heavy fibroin, and resulting mechanical properties to ascertain structure function relationships in *P. interpunctella* silk fibers. Moreover, these analyses will enable comparison to *B. mori* and other silks, natural fibers, and common polymers used in biomaterials (Table 1), which can assist in identifying future applications for *P. interpunctella* silk materials.

2. Materials and methods

2.1. Silkworm rearing and silk collection

P. interpunctella silkworms were reared at consistent environmental conditions determined previously to optimize silk production [23]. Insects were fed a standardized wheat bran diet adapted from Silhacek *et al.* [70] at 24 °C and 65 % relative humidity with a 16 hour light: 8 h dark cycle, as fully outlined in previous work [23]. In brief, 130 mg of diet was placed in the container followed by 50 mg of *P. interpunctella* eggs. Insects were reared at constant environmental conditions as the silkworms entered the 4th larval stage and began spinning silk and laying fibers along the walls of the container. Silk sheets and fiber bundles (Supplemental Fig. S1) were collected from the rearing container walls while the insects were pupating. Once adults emerged from cocoons, they were transferred to a separate container to collect eggs in order to set up new rearing containers. Adults were euthanized by freezing them for 24 hours before immediate autoclaving. Natural, un-dyed, and cut *B. mori* cocoons were obtained from Felting Supplies Store (Kitchener, Canada).

2.1.1. Silk sheet collection

Silk sheets are collected from the walls and lid of the rearing containers as previously described [23]. Silk sheets are collected once during a population life cycle, prior the emergence of moths. The majority of the silk collected is spun by the *P. interpunctella* during their 4th and 5th instar, which are the later life cycle stages of the silkworm.

2.1.2. Aligned silk fiber bundle collection

Aligned fiber bundles are collected at the same time as the silk sheets. The aligned fiber bundles, as shown in Supplemental Fig. S1, connect the top of the rearing container to the bottom of the rearing container. The average diameter of an aligned fiber bundle is consistent across rearing containers, with a average dimeter of 190–280 μm (Supplemental Table S1).

2.2. Degumming

P. interpunctella silk sheets and aligned fiber bundles were manually cleared of insect debris (food, head capsules, frass) and then boiled in ultrapure water for 15 minutes with high agitation using a magnetic stir bar (Supplemental Fig. S2). Degummed (DG) silk sheets and aligned fiber bundles were then rinsed in ultrapure water before air-drying at room temperature. *B. mori* cocoons were degummed using previously described methods [45]. Cocoons were cut into quarters and boiled in 0.04 M Na_2CO_3 (Sigma-Aldrich, USA) for 15 minutes, rinsed in ultrapure water to remove residual salt, and let air dry at room temperature in a fume hood for $>$ 48 hours. Degummed samples are used in contrast to non-degummed (NDG) samples to compare the influence of the soluble fiber coating in measured material properties.

2.2.1. Degumming in preparation for cell culture

To confirm that non-degummed and degummed samples were consistent when used for cell culture experiments, the mass of the samples following storage in water and in cell culture media was evaluated. Samples stored in cell culture media did not exhibit any mass loss (Supplemental Fig. S3).

2.3. Scanning electron microscopy

Silk fibers, aligned fiber bundles, and silk sheet samples were secured

Table 1
Mechanical and thermal properties of natural and synthetic polymers. Acronyms used: Polycaprolactone: PCL; Polyethylene terephthalate: PET; poly-L-lactic acid: PLLA; Polypropylene: PP; Polystyrene: PS; polylactic acid: PLA; Non-degummed: NDG; Degummed: DG; *Bombyx mori: B. mori; Antheraea mylitta: A. mylitta; Antheraea assamensis: A. assamensis; Philosamia ricini: P. ricini; Antheraea pernyi: A. pernyi; Samia cynthia ricini: S. c. ricini; Galleria mellonella: G. mellonella.*

Material	Tensile Modulus [GPa]	Tensile Strength [MPa]	Tg [C]	Tm [C]	Reference
Synthetic					
Nylon	2.9	71	70–158	250	[1–3]
PCL	0.21–0.44	20.7–42	−60 - −65	58–65	[4]
PET	1.25–4	51–85	85.4	254.9	[5]
PLLA	2.7–4.14	15.5–150	55–65	170–200	[4]
PP	1.4	35	−20	170	[1]
PS	3.4	49	95	240	[1]
Natural					
Bamboo	35.91	504	-	-	[6]
Chitosan	250–380	56.5–79.3	-	-	[7,8]
Collagen	0.0018–0.046	0.9–7.4	-	-	[9]
Cotton	12 ± 4	400	-	341 ± 0.4	[10,11]
Flax	60 ± 1	1100 ± 700	-	339.5 ± 0.2	[11]
Hemp	50–70	550–900	-	333.7 ± 1	[10,11]
PLA	3.1	49	50–75	140–210	[1]
Silks					
NDG B. mori	11.7 ± 2.2	635 ± 108	178–201.5	-	[12–14]
DG B. mori	12–16	700	208.7	-	[12,13]
NDG A. mylitta	-	-	237.5	-	[13]
DG A. mylitta	-	-	248.3	-	[13]
NDG A. assamensis	5.3 ± 0.4	495 ± 48	218.1	-	[12,13]
DG A. assamensis	-	-	234.2	-	[13]
NDG P. ricini	-	-	226.3	-	[13]
DG P. ricini	-	-	234.5	-	[13]
NDG A. pernyi	5 ± 0.6	426 ± 55	-	-	[12]
DG A. pernyi	8–10	517–621	-	-	[19]
NDG S. c. ricini	4.1 ± 0.6	284 ± 88	-	-	[12]
NDG G. mellonella	3.2–12.6	308.8–1270.4	-	-	[37]

to ZEISS/LEO SEM sample stubs (Ø12.7 mm x 9 mm pin height) with carbon conductive tape (Catalog No. 16202, Ted Pella, Inc., USA). Samples were dried overnight in air and sputter-coated with 8 nm of gold (ThermoFisher Scientific, USA) prior to imaging on a Phenom Pure benchtop SEM with a charge reduction sample holder. Images were obtained using a backscattered electron detector with 5 kV acceleration voltage for imaging and analysis. Long axis fiber diameter measurements of non-degummed and degummed *P. interpunctella* and *B. mori* silk fibers were completed in ImageJ analysis software (US NIH, USA) across 3 different samples and 3 representative images from each sample (n = 90). Diameters of aligned fiber bundles and silk sheet thickness measurements for non-degummed and degummed *P. interpunctella* samples were completed in ImageJ to determine cross-sectional areas for rheological assessments.

2.4. Fourier transform infrared (FTIR) spectroscopy

Silk fibers were analyzed using attenuated total reflectance (ATR) with a zinc selenide crystal on a Nicolet iS50 FTIR Spectrometer (ThermoFisher Scientific, USA) (UF Nanoscale Research Facility). Spectra was collected over 64 scans at a resolution of 4 cm^{-1} over a 4000–650 cm^{-1} wavenumber range for non-degummed and degummed silk (n = 6). Background spectra were collected at the same conditions to be subtracted from the sample spectra in OMNIC™ Spectra Software and then analyzed with Origin data analysis software (OriginLab Corporation, USA). Deconvolution of the secondary structure was performed within the amide I region (1590–1720 cm^{-1}) according to Hu *et al.* [15] to estimate protein secondary structure. Peaks are correlated to secondary structures as follows: 1605–1615 cm^{-1} as side chains, 1616–1637 cm^{-1} and 1697–1703 cm^{-1} as β-sheet structures, 1638–1655 cm^{-1} as random coils, 1656–1662 cm^{-1} as α-helical bands, and 1663–1696 cm^{-1} as turns.

2.5. Protein sequence assessments in Geneious®

The Stoppel lab maintains licenses to Geneious® software to assist in gene and protein sequence assessments. The tools within the software are used to aid in understanding of secondary structures within silk fibroin heavy chain protein sequences as well as calculate standard properties such as molecular weight, isoelectric points (pI), to calculate sequence prevalence. EMBOSS 6.5.7 and the Garnier tool were used to predict secondary structures within the protein sequence to understand what amino acid sequences can lead to the various secondary structures measured with FTIR spectroscopy. Complete information for sequences referenced in this manuscript is given in Supplemental Table S2. In this manuscript, amino acids are represented by their standard single letter abbreviation and the letter X is used to represent any amino acid or specific amino acids as noted in Supplemental Table S2. Files used for raw data are found here: *B. mori*: NP_001106733.1 FASTA file and *P. interpunctella*: XP_053613783.1 fasta file.

2.6. Thermal gravimetric analysis

Degradation behavior of *P. interpunctella* silk was analyzed using TA Instruments TGA550 (TA Instruments, USA). Samples (5–10 mg) were placed in platinum pans (TA Instruments, USA, 957207.904) and ramped from ambient temperature to 800 C at 10 C/min with air flow of 40 L/min and N_2 flow of 60 L/min. Mass loss curves are normalized to total sample mass after water evaporation at 100 ℃ and are represented as an average curve ± standard deviation. Water content, T_{onset}, and T_d were determined using TA Instruments TRIOS® analysis software.

2.7. Differential scanning calorimetry

Standard mode DSC analysis of thermal transitions of *P. interpunctella* silk was completed using a TA Instrument DSC250 (TA Instruments, USA). Samples (10 mg) were pressed into aluminum Tzero pans (TA Instruments, USA, 901683.901) and ramped from 0 to 300 ℃ at 10 ℃/

min with a purge gas (N_2) flow of 50 L/min. Heat-cool cycles were performed by heating samples from −50–180 ℃ and cooling from 180 to −50 ℃ at a constant rate of 10 ℃/min, repeated 2 times. Temperature modulated DSC measurements were completed on a TA Instruments DSC2500 (TA Instruments, USA). Modulation was performed on non-degummed and degummed silk samples sealed in Al Tzero pans at a modulation period of 60 seconds, temperature amplitude of 0.3 ℃, and heating rate of 2 ℃/min with a N_2 flow of 50 L/min. Thermal transitions were analyzed using TA Instruments TRIOS analysis software.

2.8. Bulk extensional mechanical properties

The diameters of the aligned fiber bundles and thickness of silk sheets were measured via SEM (Supplemental Table S1). Aligned fiber bundles and silk sheets were secured to thin paper frames at their ends to prevent slipping in the instrument. The gauge length of all samples prior to tensile testing was 10 mm. The width of the sheets was also 10 mm. The samples in the paper frames were inserted into the solid rectangular fixture (SRF) screw clamps of an Anton Paar MCT 702e Rheometer (Anton Paar, Graz, Austria) equipped with twin drive motors for dynamic mechanical analyzer (DMA) capabilities. The sample in the paper frame was tightened in the clamps to 10 centinewton/meter with a torsion screwdriver. Once the sample was secured, the side paper panels were cut with scissors. The sheet samples were inserted into the clamps and tightened to 10 centinewton/meter. Anton Paar RheoCompass software was used to pre-stretch the samples to 0.1 N and perform static extensional tests at 1 mm/min and 10 mm/min strain rates. The Young's modulus (E), ultimate tensile strength (UTS), and maximum strain (ε_{max}) were calculated from the resulting stress-strain curves.

2.8.1. Bulk extensional mechanical properties of silk sheets in water and cell culture media

Supplemental Fig. S4 shows the experimental set-up for the bulk mechanical assessments of silk sheets. **Supplemental Video S1** shows an example test run. Evaluation of these materials in serum-containing media was also performed to ensure cell culture results were impactful, as described in **Supplemental Section 3.1** and Supplemental Fig. S5 show the experimental setup and conditions. Standard cell culture media was used with a recipe of Dulbecco's Modified Eagle's Medium (DMEM, ThermoFisher Scientific USA) supplemented with 10 % fetal bovine serum when appropriate (FBS, ThermoFisher Scientific, USA) and 5 % penicillin-streptomycin (ThermoFisher Scientific, USA).

Supplementary material related to this article can be found online at doi:10.1016/j.mtcomm.2024.111416.

2.8.2. Bulk extensional mechanical properties of aligned fiber bundles

Supplemental Fig. S6 shows the experimental set-up for the bulk mechanical assessments of silk sheets. **Supplemental Video S2** shows an example test run. The fracture of the aligned fiber bundles during extensional testing are shown in Supplemental Fig. S7 and the calculation of the pore size and void space between the figures are shown in Supplemental Fig. S8. Discussion of these data are given in **Supplemental Section 4.**

Supplementary material related to this article can be found online at doi:10.1016/j.mtcomm.2024.111416.

2.9. Atomic force microscopy

Individual silk fibers were secured to glass slides and scanned in air on a Nanowizard 4XP ZEISS LSM 900 AFM (Bruker, GER) in QI Advanced Imaging mode. Height images and force spectroscopy maps were performed with a FESP V2 cantilever (8 nm nominal tip radius, k = 2.8 N/m, f = 75 kHz) (Bruker, USA, FESP-V2-FESP-V2) calibrated on glass slides prior to scanning. Images for analysis were captured over a 0.5 μm x 0.5 μm scan area (256 ×256 pixels) at a z-length of 200 nm and 5–10 nN setpoint. Scans were collected on 4 fibers (n = 4) with 3 scans per fiber (N = 3) to account for biological variability and instrumental noise, respectively. Young's modulus (E_{fiber}) and the adhesive force between the tip and the sample was extracted from each force curve in Bruker JPK SPM processing software. Sample calculations are shown in Supplemental Fig. S9. Assessment of sample variability is shown in Supplemental Fig. S10. Measured parameters are reported as the mean ± standard deviation from the average E_{fiber} and adhesion for each individual fiber. Reported averages and standard deviation for E_{fiber} were calculated after gating data between 10 MPa and 10 GPa to account for issues resulting from inaccurate curve fitting. For comparison, data were collected for *B. mori* cocoon silk fibers and are discussed in **Supplemental Section 5.1** and shown in Supplemental Fig. S11.

2.10. NHLF culture and cell proliferation assays

Normal human lung fibroblasts (NHLF) were purchased from Lonza Walkersville, Inc. (Walkersville, MD). NHLFs passage 11–14 were cultured at 37 ℃ with 5 % CO_2. Standard cell culture was conducted using Dulbecco's Modified Eagle's Medium (DMEM, ThermoFisher Scientific USA) supplemented with 10 % fetal bovine serum (FBS, ThermoFisher Scientific, USA) and 5 % penicillin-streptomycin (ThermoFisher Scientific, USA) for samples tested with FBS. Cell culture was conducted using DMEM supplemented with 5 % penicillin-streptomycin for experiments without FBS. Culture media was changed every 2 days. Metabolic activity was assessed using either media with or without FBS for comparison of FBS passive adsorption onto the silk fibers as discussed in **Supplemental Section 6** and data are normalized to samples grown on tissue culture plastic (Supplemental Fig. S12 and Supplemental Fig. S13). Samples were prepared from clean, non-degummed and degummed *P. interpunctella* silk sheets that were sterilized by autoclaving (120 ℃ and 0.101 MPa) prior to cutting 10 mm diameter samples with a biopsy punch. Non-degummed and degummed *P. interpunctella* silk samples (NDG *Pi* and DG *Pi*, respectively) were placed in 48-well plates and secured with Teflon O-rings (OD ¼ in. ID, 3/8 in., Lamons, USA) before NHLFs were seeded at a density of 30,000 cells/cm^2 in concentrated droplets, less than 150 μL. Well plates were incubated for 30 minutes before addition of culture media until a total volume of 200 μL per well was achieved. Metabolic activity was detected after 1 and 3 days of culture using AlamarBlue (ThermoFisher Scientific, USA) according to the manufacturer's instructions. Briefly, culture media was aspirated from each sample and replaced with 180 μL of culture media and 20 μL of AlamarBlue solution. After 1 hour of incubation at 37 ℃, 100 μL of each sample was transferred to a white walled 96-well plate where the absorbance (n = 7) in each well was measured at 570 nm (n = 3) on a BioTek Synergy H1 Microplate Reader (Winooski, USA). The background absorbance was accounted for using DMEM. Relative metabolic activity was obtained by dividing each sample's metabolic activity by the average tissue culture plastic absorbance corresponding to the appropriate time point (control metabolic activity = 1).

2.11. Fluorescence microscopy

NHLFs were cultured at 37 ℃ with 5 % CO_2 for 1 and 3 days on non-degummed and degummed *P. interpunctella* silk before being fixed with 10 % phosphate buffered formalin (ThermoFisher Scientific, USA) at room temperature for 10 minutes. Samples were washed 3 times with phosphate buffered saline 1X (PBS, ThermoFisher Scientific, USA) before permeabilization with 0.05 % Triton X-100 (v/v in PBS, ThermoFisher Scientific, USA) for 15 minutes. Following permeabilization, samples were washed with PBS 3 times before being blocked with 5 % donkey serum in 1 % bovine serum albumin (BSA) overnight at 4 ℃. To counteract the strong autofluorescence signal that silk fibers exhibit, samples were incubated with 10 μg/mL Sudan Black B counterstain (ThermoFisher Scientific, USA) dissolved in 70 % ethanol (ThermoFisher Scientific, USA) for 20 minutes at room temperature in the dark as

described previously [71,72]. The counterstain solution was removed and replaced with 200 μL of 1 % BSA. Samples were then incubated for 4 hours with 8 μL (10 μg/mL) of Alexa Fluor 488 Phalloidin (ThermoFisher Scientific, USA) at room temperature in the dark while rocking. 6-diamidino-2-phenylindole (DAPI, ThermoFisher Scientific, USA) was added to each well in 10 μL aliquots (12 μg/mL) for 30 minutes at room temperature and then samples were thoroughly washed in PBS-T before mounting onto glass slides using glycerol (ThermoFisher Scientific, USA) and a glass coverslip. Images were captured and processed on a Keyence BZ-X800 microscope.

2.12. Statistical methods

Experimental data are primarily expressed as average ± standard deviation with a minimum n = 3. GraphPad Prism 10.2.1 (GraphPad Software Inc., USA) was used for statistical analysis. Analysis was performed with appropriate-size analysis of variance (ANOVA) with Tukey's test post-hoc analysis. Statistical significance is reported as $*p< 0.05$, $**p< 0.01$, $***p < 0.001$, and $****p < 0.0001$ with key features shown in the figures and tables and further information provided in the supplemental information as noted throughout the methods section. Specifics on the statistical test, p values, and definition of n are all present in individual figure and table captions.

3. Results and discussion

The results presented herein explore the functional properties of *P. interpunctella* silk in the context of other polymers (Table 1) and as a raw material for environmental and biomedical applications. *P. interpunctella* silk fiber structure and composition and, more specifically, silk fibroin heavy chain, is expected to have observable differences in material characteristics from other relevant polymers in biomaterial applications (Fig. 1). For applications where a purified polymer system is required (e.g., medicine), enrichment of silk fibroins through degumming processes is utilized to lessen variability in silk material properties and prevent immune reactions when a material is implanted. This manuscript builds upon work that previously degummed *P. interpunctella* silk [23] by evaluating how the removal of silk fiber coating proteins, such as sericins, impacts material characteristics and cytocompatibility to expand on perspectives of *P. interpunctella* silk as a raw material source for biomaterial development.

Throughout the manuscript, raw *P. interpunctella* silk fibers (non-degummed, NDG) are compared to enriched or degummed silk fibers (degummed, DG). Multiple conditions of degumming were evaluated to determine the optimal temperature and time conditions that lead to isolation of *P. interpunctella* silk fibroin (Supplemental Fig. S2). *P. interpunctella* silk degummed in boiling ultrapure water for 15 minutes shows complete removal of visual web-like structures with a 45–55 % mass loss, attributed to the absence of sericin proteins and aligning with findings from Shirk *et al.* [23]. Across all assessments, non-degummed fibers are compared to degummed fibers to provide conclusions relevant to the raw material and to potential translation of *P. interpunctella* silk biomaterials to the medical field.

3.1. Morphology and protein structure of P. interpunctella silk fibers

To begin to evaluate *P. interpunctella* silk for silk-based biomaterials, *P. interpunctella* silk fiber morphology and structure is first compared to that of *B. mori* silk. *B. mori* silk is the most extensively studied silk source in silk-based biomaterial research, largely due to the commercial availability of silk cocoons and previous applications extending from silk textiles. Scanning electron microscopy imaging of non-degummed and degummed silk sheets and cocoons from *P. interpunctella* and *B. mori* silkworms was used to visualize characteristic silk structures and assess changes in the raw material morphology as a function of degumming processes and insect type.

Representative SEM images of fibers within *P. interpunctella* silk sheets and *B. mori* cocoons clearly show the significant difference in fiber size between the two insects (Fig. 2**AB**). Fibers from *P. interpunctella* (Fig. 2**C**) are considerably smaller than *B. mori* (Fig. 2**D**),

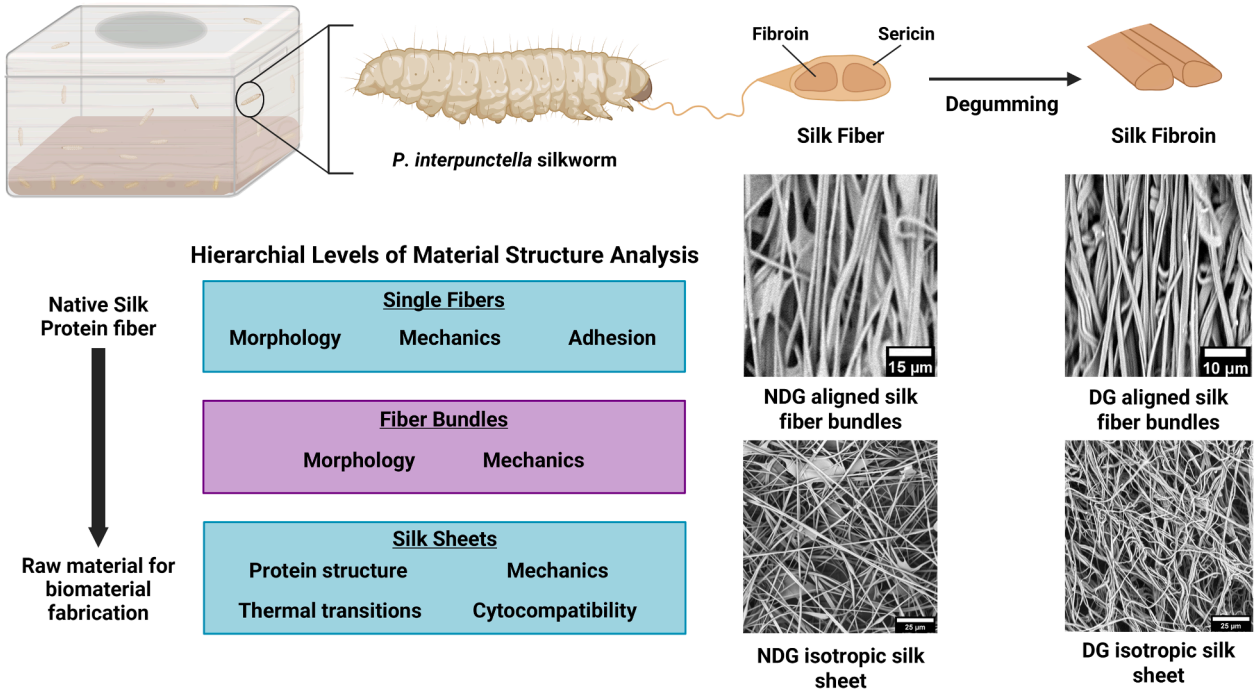

Fig. 1. Levels of material properties of *P. interpunctella* silk evaluated in this manuscript. *P. interpunctella* larva grown in the laboratory produce individual silk fibers that accumulate naturally in their rearing containers over their life cycle into complex 3D structures (fiber bundles, silk sheets), enabling more extensive analysis of material properties. Assessments of silk fiber morphology, adhesive forces, protein secondary structure, thermal stability, mechanical properties, and cytocompatibility are completed through the study of non-degummed (NDG) and degummed (DG) single fibers, aligned fiber bundles, and silk sheets.

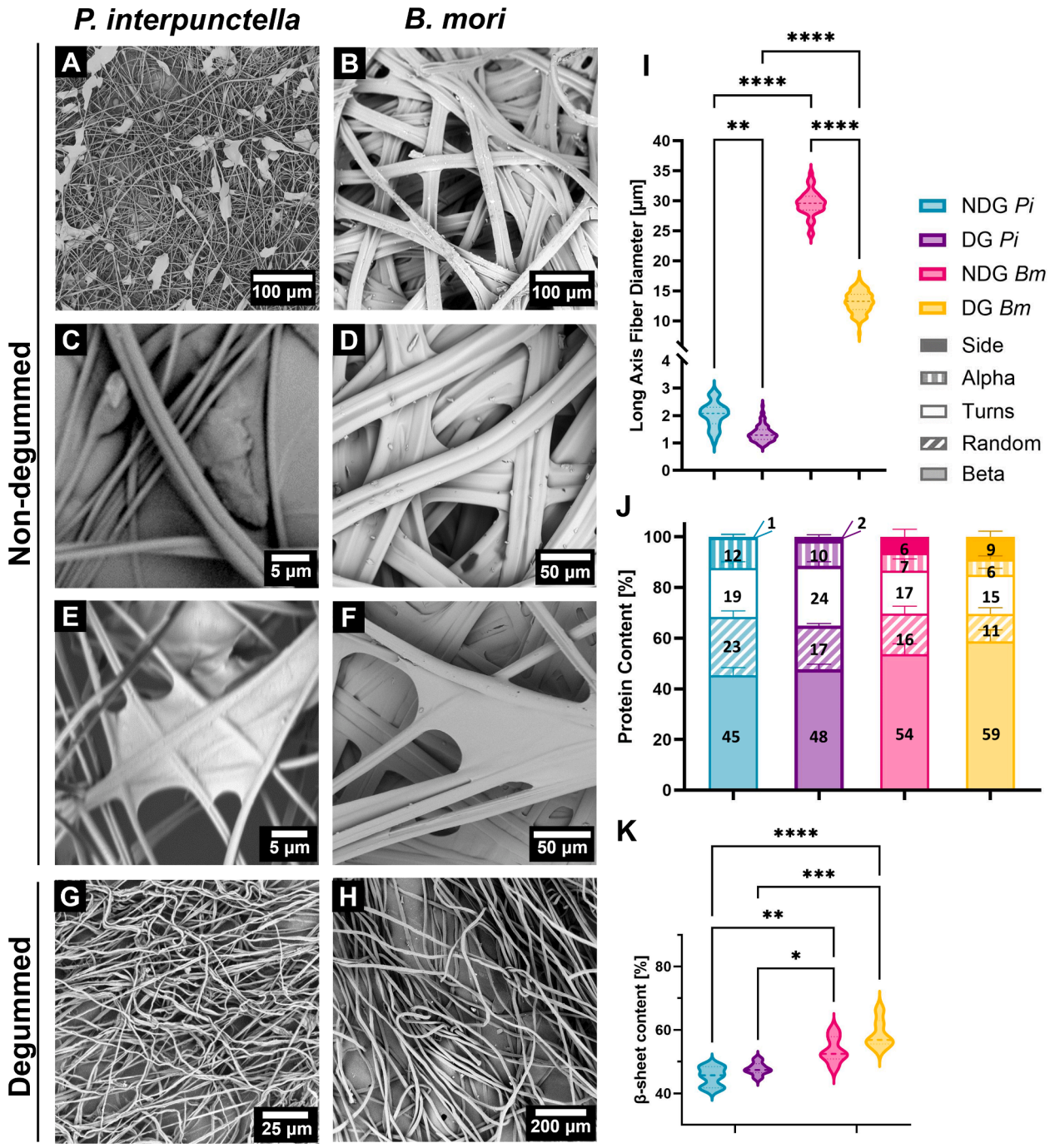

Fig. 2. Fiber structure of non-degummed (NDG) and degummed (DG) *P. interpunctella* (*Pi*) and *B. mori* (*Bm*) fibers. Representative SEM images of non-degummed *P. interpunctella* silk sheet (**A**) and *B. mori* cocoon (**B**), *P. interpunctella* (**C**) and B. mori (**D**) single fibers, and *P. interpunctella* (**E**) and *B. mori* (**F**) sericin-like structures. SEM images of *P. interpunctella* (**G**) and *B. mori* (**H**) fibers degummed for 15 minutes showing removal of web-like structures. (**I**) Long axis fiber diameters for non-degummed and degummed silk fibers (n = 90) (**J**) Relative protein content and (**K**) β-sheet content of non-degummed and degummed silk fibers (n = 6) determined through deconvolution of the amide I peak using methods reported by Hu *et al.*[15]. Data are expressed as mean ± standard deviation. Analyzed with 2-Way ANOVA with Tukey's test post-hoc analysis. Statistical significance is reported as *p < 0.05, **p < 0.01, ***p < 0.001, and ****p < 0.0001.

with long-axis fiber diameters of 2.1 ± 0.5 µm for *P. interpunctella* and 29.6 ± 2.1 µm (n = 90) for *B. mori*, (Fig. 2**I**). Variability in fiber diameter within insect type can stem from biological variability between silkworms and, in the case of *P. interpunctella*, that the silk sheets are an accumulation of many individual fibers laid between the 4th-5th instar phases, meaning fibers are an accumulation of materials produced by many *P. interpunctella* silkworms at later life stages compared to a *B. mori* cocoon, which is produced by a single insect at the pupal life stage.

Biologically, the difference in size between *P. interpunctella* and *B. mori* fibers is primarily due to the difference in insect size, as *B. mori* is a much larger silkworm (~40 mm) than *P. interpunctella* (~12–14 mm) and the insects possess different biological limits as result. Despite this difference in size, *P. interpunctella* fibers maintain the double-stranded structure of *B. mori* and other silkworm fibers, characteristic of two fibroin brins surrounded by an outer coating layer comprised, of sericins and less well-characterized proteins (*e.g.,* mucins, seroins), originating from the two silk glands within the insects (**Fig. 2CD**). An important observation is the appearance of irregularly shaped, web-like structures

connecting *P. interpunctella* fibers in the silk sheets (Fig. 2**A**), further visualized in Fig. 2**E**, in addition to debris from the insect. These webbed structures are hypothesized to be similar to the web-like sericin-based coatings between *B. mori* cocoon fibers or sericin sheets observed in *Galleria mellonella* (*G. mellonella*) silk [37] (Fig. 2**F**). These structures could also contain secretions from the mandible, Filippi, or salivary glands, though the existence and role of these glands in silk production varies across lepidopteran organisms [73–75]. Visualization of debris in the silk sheet and large globular structures raises the consideration of methods to remove these impurities, in the case that they would lead to unfavorable interactions or variability in a biomaterial format. To explore this, *P. interpunctella* and *B. mori* fibers were degummed for 15 minutes, as this showed complete removal of web-like structures when imaged (Fig. 2**GH**). Both *P. interpunctella* and *B. mori* silk displayed significant decreases in fiber diameter upon degumming, which confirms that employed degumming processes were successful in the removal of the outer coating. Further evaluation of degumming processes may be necessary to fully confirm complete removal of the outer coating. However, this is challenging at this stage of *P. interpunctella* research and silk fiber research in general, as the composition of the coating is not fully understood.

Given the reported differences in silk fibroin heavy chain gene sequences and protein structures between *B. mori* and *P. interpunctella* (expanded on by Wu et al. [69]), the relative protein structure of *P. interpunctella* and *B. mori* silk fibroin was further evaluated through FTIR. Protein secondary structure, specifically the content of β-sheet structures, is highly influential in silk fiber and silk biomaterial properties. Crystallinity of the silk/silk fibroin protein is consistently studied throughout silk fiber and silk biomaterial research; however, it has not been established for *P. interpunctella* silk outside of the analysis of the silk fibroin heavy chain protein sequence [68,69,76]. *P. interpunctella* FTIR spectra exhibits the characteristic amide I, II, and III peaks found in silk proteins (see Supplemental Fig. S14). Through previously reported deconvolution methods [15] for the amide I peak, the relative content of β-sheet, random coils, turns, α-helix, and side chain secondary structures in the *P. interpunctella* silk fibroin protein is estimated (Fig. 2**J**). Non-degummed *P. interpunctella* silk fibers (blue) possess lower β-sheet content relative to non-degummed *B. mori* (pink) silk fibers ($p < 0.01$, $n = 6$), with higher levels of α-helices, turns, and random coils. Relative β-sheet content of non-degummed *B. mori* (54 %) and degummed *B. mori* silk (59 %) fall within ranges reported previously for *B. mori* silk wastes and degummed cocoons (53–65 %) [77]. An additional representation of these results can be found in Supplemental Fig. S15. These differences in β-sheet content align with previous reports of *P. interpunctella* silk fibroin protein sequence analyses [69], wherein there is more repeat irregularity as well as potential crystalline regions resulting from other amino acid sequences. Degumming of *P. interpunctella* silk fibers did not significantly shift protein structure, though statistical significance remained between degummed *P. interpunctella* (purple) and *B. mori* silks (yellow) ($p< 0.001$). The results from the two-way ANOVA show that the insect type has a greater statistically significant influence ($p< 0.0001$) on β-sheet content compared to removal of the sericin coating through degumming processes ($p< 0.05$). These measured differences in crystallinity through silk fibroin protein sequence and degumming are expected to be apparent in thermal and mechanical assessment as well since silk fibroin is the primary driver of silk fiber properties.

3.1.1. Perspectives on the role of protein sequence in observed secondary structures of P. interpunctella silk fibers

Analyses and annotation of the *P. interpunctella* heavy chain silk fibroin gene suggest that the protein should have a molecular weight around ~390 kDa and possess a high percentage of charged amino acid residues. Deeper investigations into *B. mori* over the last 20 years have shown that amino acid composition, sequence, and resulting secondary structures drive *B. mori* silk fibroin properties [68,69,76,78]. The silk fibroin heavy chain protein sequences between *P. interpunctella* and *B. mori* are not very similar, as aligning the proteins (*B. mori*: NP_001106733.1 FASTA file and *P. interpunctella*: XP_053613783.1 fasta file) in Geneious® yields only 27 % sequence alignment. This suggests that the secondary structures that arise in *P. interpunctella* may vary from the specific protein sequences implicated in *B. mori* secondary structure formation. In *B. mori*, protein sequences such as GAGAX, GSGAX, or SGAGAGX are responsible for β-sheet formation [21,79] and account for 73 % (GAGAX, SGAGAGX) and 55 % (GSGAX) of the total molecular weight of the *B. mori* fibroin heavy chain. Sequence assessments (Supplemental Table 2**)** show that in these *B. mori* β-sheet structures, the X or unknown protein is often G, Y, or V, which are hydrophobic or uncharged polar amino acids.

Consequently, sequences that may yield additional β-sheet structures within the fibroin heavy chain sequence in *P. interpunctella* can be found in insects more closely related based on phylogenetic analyses. *P. interpunctella* shows 53 % alignment of protein sequences with *Ephestia kuehniella* (WDD44661.1 FASTA file) and 41 % alignment with *Galleria mellonella* (XP_026760882.2 FASTA file), when assessed in Geneious®. Zurovec and his team have shown similar results in their work, suggesting that repeat motifs such as VIVIX or XVIVI in *E. kuehniella* and *G. mellonella* are conserved hydrophobic repeat regions [69]. Further analysis of the *P. interpunctella* fibroin heavy chain in Geneious® suggests the PVVIIEX and XVVVIX sequences may yield β-sheet structures, with 26 and 4 of these sequences found in the *P. interpunctella* heavy chain, respectively. In all cases, these PVVIIEX or XVVVIX sequences are followed by a XAAAAX sequence (alanine-rich region) that accounts for approximately 5 % of the total molecular weight of the *P. interpunctella* silk fibroin heavy chain protein. These calculations and assessments are presented in Supplemental Table 2. *P. interpunctella* heavy chain silk fibroin yields common repeating sequences such as GASX, GASXASAX, and GAVGAX, which respectively account for just 9 %, 14 %, and 1 % of the *P. interpunctella* molecular weight. This means secondary structures similar to *B. mori* only make up a portion of the β-sheet structures measured within *P. interpunctella* silk fibers. Taken together, the GASXASAX, GAVGAX, and PVVIIEX/XVVVIX + XAAAAX sequences account for 27 % of the molecular weight of the *P. interpunctella* silk fibroin heavy chain protein. While this does not fully explain the 48 % β-sheet content measured by FTIR spectroscopy in (Fig. 2**J**), it confirms that the protein sequences that yield β-sheet structures in *P. interpunctella* are different from those in *B. mori*, as expected based on prior investigations [21,69,79]. These differences could be due to other unidentified amino acid sequences that contribute to the β-sheet content or the other proteins present in the fiber (e.g., the fiber coating, silk fibroin light chain) could also contribute to the FTIR results.

Moving forward, the most important part of this discussion is that this change in sequence to structure between *P. interpunctella* and *B. mori* may also yield a change in polymer function. *P. interpunctella* silk fibroin may have different properties when it comes to kinetically trapping and stabilizing bioactive molecules or may have different properties when it comes to regenerating and reconfiguring the protein to produce new material structures, as commonly done with *B. mori* silk fibers [45,80]. This necessitates further characterization of resulting *P. interpunctella* silk fibroin solutions and their use in biomedical or environmental applications, which is outside the scope of this manuscript. Herein, the aim is to better contextualize raw and degummed *P. interpunctella* silk fibers, comparing *P. interpunctella* silk fiber properties to a wide range of natural and synthetic fibers for the remainder of this manuscript, highlighting potential applications for these materials.

3.2. Thermal properties of P. interpunctella silk

One way to understand how crystal structure manifests in material stability is to analyze the fiber and protein responses during thermal decomposition. Thermal gravimetric analysis (TGA) of non-degummed

and degummed *P. interpunctella* sheets was performed to investigate material degradation (n = 3). Data shown in Fig. 3**A** is represented as the average ± standard deviation after normalizing the remaining mass % to the sample mass after evaporation of absorbed water at 100 ℃. Samples experienced mass loss between 5 % and 8 % at 100 ℃, attributed to the moisture content originally present in the sample; differences in water content between non-degummed and degummed *P. interpunctella* was not statistically significant. Silk samples experienced rapid mass loss as the fiber began degrading, with the onset of degradation beginning around 235 and 265 ℃ for non-degummed and degummed silk, respectively. Similar trends were reported in silk fiber assessments from other species (*B. mori, A. mylitta, A. assamensis, P. ricini*), [13] potentially due to a reduced molecular mass of the silk protein or a disruption in inter-molecular protein interactions during the degumming and fiber preparation processes. As *P. interpunctella* silk was degummed in boiling water, it is possible that the polymer chain experienced thermal stress that began to degrade or shorten the polymer, modifying the molecular mass distribution of the sample and thermal properties. This modification of polymer chain length through degumming has been seen in processing of *B. mori* silk into silk polymer solution, wherein increasing or decreasing the degumming time of the silk can tune the molecular mass distribution of silk fibroin in the solution [44,81]. This tunability could potentially be applied to *P. interpunctella* silk to achieve a range of thermal and mechanical properties of the fiber, but full investigation of these hypotheses is outside of the scope of these initial characterizations.

To further evaluate these materials, the thermal transitions of non-degummed and degummed *P. interpunctella* silk were analyzed through differential scanning calorimetry. Fig. 3**B** shows a lower temperature transition between 20 and 30 ℃ in both non-degummed and degummed *P. interpunctella* silk, with a small shoulder on the degummed peak following the transition (purple). This early melting and crystallization behavior is hypothesized to be correlated to the presence of sericins or outer coating proteins. This peak corresponds to similar to DSC analysis of *B. mori* silk gland contents which attributed low temperature transitions between 40 and 45 ℃ to sericins [82]. This transition behavior is conserved through repetitive heat-cool cycles, further visualized in Supplemental Fig. S15A, highlighting the early melting behavior upon heating and crystallization upon cooling in *P. interpunctella* silk after surface-bound water is removed. The observation of this low temperature transition in degummed silk samples could result from residual sericins that were not completely removed from the silk fiber sheets during degumming. While it is not the current focus of this study, future work will aim to expand on the extent to which *P. interpunctella* silk fibroin is purified through degumming time, as ongoing efforts aim to process *P. interpunctella* silk into biomaterial formats.

There is no significant shift in the bound water evaporation peak between non-degummed and degummed silk (85–95 C), which agrees with the similar water content observed between non-degummed and degummed sheets through TGA. Non-degummed *P. interpunctella* silk exhibited melting-like behavior around 247 ℃ prior to degradation between 270 and 300 ℃, aligning with degradation behavior observed in TGA (Fig. 3**A**). Comparisons of the melting point of *P. interpunctella* silk to other silk fibers is limited due to issues resulting from protein degradation obscuring melting behavior [13,83]. However, the observed T_m of non-degummed *P. interpunctella* silk is expected to be lower due to differences in silk fibroin sequence and structure. Degummed *P. interpunctella* silk did not have an observable melting point prior to degradation, which is similar to observations reported for non-degummed *B. mori*, *A. mylitta*, *A. assamensis*, and *P. ricini* silks [13], but could also result from the heat treatment during degumming. Observations of silk sheet and fiber bundle cross-sections after degumming show condensed, more dense morphology of the bulk material and flattened individual fiber cross-sections (Supplemental Fig. S2). It is possible that, along with a visual shift in fiber morphology, degumming also modifies the structure, stability, or interactions between the proteins in *P. interpunctella* silk fibers, causing a more gradual transition of polymer chain disentanglement between the solid and liquid melt phase that is not observable through standard DSC. Lower thermal properties observed in *P. interpunctella* silk (summarized in Fig. 3**C**) is expected to correspond to lower tensile strength and elastic modulus, due to differences in molecular mobility and stiffness resulting from reduced β-sheet content of *P. interpunctella* silk (shown in Fig. 2**K**).

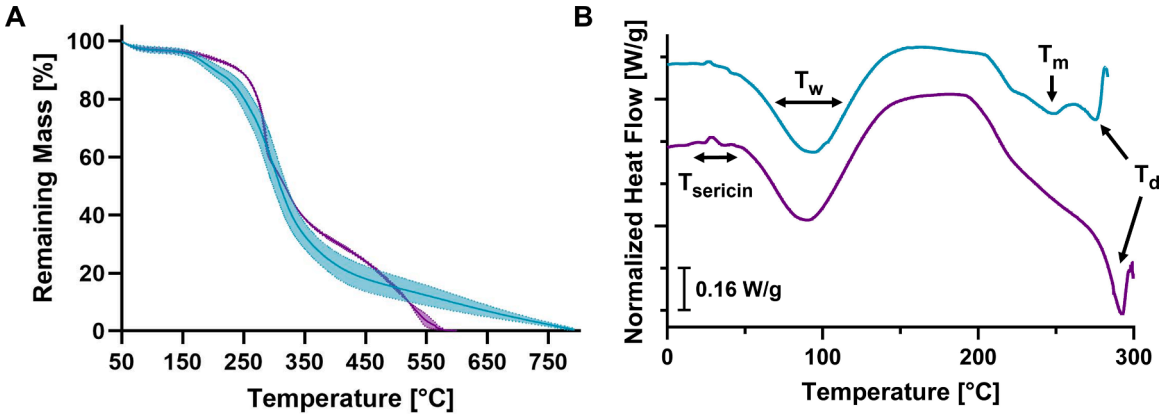

C

Sample	T_g [°C]	T_m [°C]	$T_{d,onset}$ [°C]	T_d [°C]
NDG *Pi*	150-170	247.4 ± 1.6	234.1 ± 3.8	293.9 ± 0.2
DG *Pi*	-	-	265.2 ± 1.5****	284.4 ± 1.9**

NDG *Pi*
DG *Pi*

Fig. 3. Thermal properties of *P. interpunctella* (*Pi*) silk sheets. (**A**) TGA curves of non-degummed (blue) and degummed (purple) silk sheets. Data are expressed as mean ± standard deviation (n = 3). (**B**) DSC curves of non-degummed and degummed silk sheets. Temperature transition regions related to sericins ($T_{sericin}$), bound water (T_w), melting (T_m), and material degradation (T_d) are labeled. (**C**) Thermal transition temperatures of *P. interpunctella* silk determined by TGA and DSC. Data are expressed as a range from onset to end (n = 1) or mean ± standard deviation (n = 3). Analyzed with 1-Way ANOVA with Tukey's test post-hoc analysis. Statistical significance is reported as **p < 0.01 and ****p < 0.0001.

3.3. Mechanical properties of *P. interpunctella* silk materials

In silk literature it has been hypothesized that the mechanical response of the material is directly related to the protein content and resulting secondary structure, with emphasis given to the frequency of the repeat unit structure correlating to mechanical strength [55,68,76]. Short motifs with irregular spacing are not able to have as many interactions as compared to a longer more repetitive repeat unit, resulting in possibly a poorly organized and weak material [76]. More repetitive units that contribute to β-sheet formation have the ability to generate large crystalline structures that are rigid but very strong [21,76]. Recently, it has been shown through molecular dynamics simulations of silk fibroin from *B. mori* that larger crystalline regions result in more robust, but brittle materials [40]. While smaller crystalline regions broken up by more flexible side chains provide more elastic properties and an increased viscoelastic response [40]. In *P. interpunctella*, it is hypothesized that the decrease in β-sheet content (Fig. 2**K**), as compared to other silk fibroins like *B. mori* [76], and the spacing between *P. interpunctella* silk fibroin repeat units, will produce a more linear, viscoelastic response, correlating to an increase in Young's modulus, but a decrease in UTS.

Previous work characterizing *P. interpunctella* has been limited in methodology and sample size. Fedic *et al.* performed extensional testing on individual fibers to identify differences in protein composition and organization to mechanical response [76]. Shirk et al. performed a limited extensional study of *P. interpunctella* sheets to determine the impacts of rearing conditions on mechanical response of the insect's raw silk [23]. This manuscript builds upon previous assessments with improved reproducibility and sample size for different structural levels of analysis. Bulk tensile mechanical assessments were performed on non-degummed and degummed silk sheets collected from the *P. interpunctella* insect rearing containers. Bulk tensile assessments were also performed on aligned fiber bundles using static testing via DMA to determine the impact of anisotropy on *P. interpunctella* silk. Local mechanical property assessment was used to determine modulus of single fibers as well as adhesion properties via AFM.

3.3.1. Bulk mechanical properties of *P. interpunctella* silk sheets

Bulk mechanical assessment was performed on non-degummed and degummed *P. interpunctella* sheets (n = 6) collected directly from the rearing vessels. The sheets were attached to paper frames with a uniform gauge length of 10 mm (Supplemental Fig. S4A). Stress-strain curves were collected at two different strain rates of 1 mm/min (squares) and 10 mm/min (circles) to determine the effect of strain rate and processing conditions on the silk sheets. An example extensional test at 10 mm/min can be seen in **Supplemental Video 1**. Representative stress-strain curves (Fig. 4**A**) demonstrate an elastic response as low strain (<0.05 mm/mm) and a plastic, mostly brittle or ductile response at high strains (>0.2 mm/mm). The non-degummed (blue) *P. interpunctella* sheets produce a strain-stiffening response until they reach their ultimate tensile strength (3.75 ± 1.5 MPa, 10 mm/min), where they then experience a brittle response, with some ductile breakage, and then full rupture. The degummed (purple) *P. interpunctella* sheets produce a strain stiffening response with a much larger stress response than the non-degummed sheets. The degummed sheets produce a ductile response where their full rupture occurs well after the UTS_{sheet} (8.15 ± 3.2 MPa, 10 mm/min) and strain-weaking response at high strain.

Young's modulus (E_{sheet}), UTS_{sheet}, and maximum strain ($\varepsilon_{max,sheet}$) were all calculated from the stress-strain curves (Supplemental Fig. S4) and averages can be found in Supplemental Table 1. The effect of degumming the sheets showed significant differences in E_{sheet} (Fig. 4**B**) at a rate of 1 mm/min (lighter color points), but no significant difference at 10 mm/min (darker color points). Young's modulus of non-degummed sheets showed lower standard deviation than the degummed sheets, suggesting that the degumming may be incomplete or variable in its impact on the fiber structure and composition. There exists marginal statistical significance ($p = 0.0188$) in the degummed sheets between the two different strain rates, demonstrating that the mechanical properties of *P. interpunctella* sheets are strain rate dependent. However, the results from the two-way ANOVA statistical analysis show

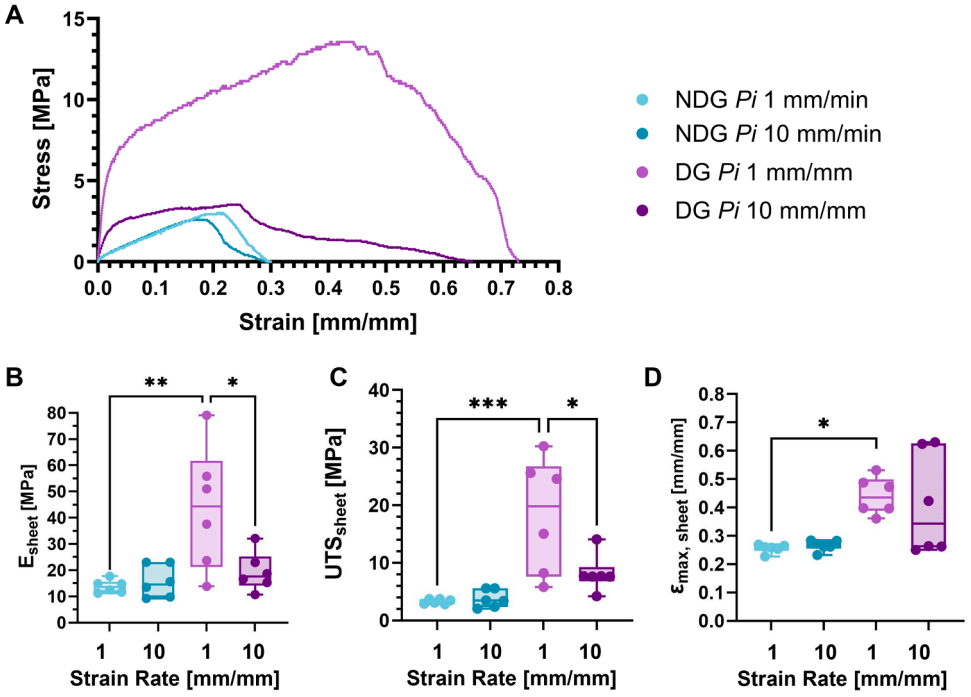

Fig. 4. Static tensile testing of *P. interpunctella* (*Pi*) sheets at 1 mm/min (lighter color) and 10 mm/min (darker color) strain rates (**A**) Representative stress-strain curves for non-degummed (NDG, blue) and degummed (DG, purple) *P. interpunctella* sheets (**B**) Young's modulus (n = 6) (**C**) Ultimate tensile strength (n = 6) and (**D**) strain at max elongation (n = 6). Data are expressed as mean ± standard deviation. Analyzed with 2-Way ANOVA with Tukey's test post-hoc analysis. Statistical significance is reported as *p < 0.05, **p < 0.01, and ***p < 0.001.

that the degumming process has a larger statistically significant effect (p= 0.0045) on the E_{sheet} than changing the strain rate (p = 0.0463). These trends are also held for the UTS_{sheet} (Fig. 4**C**). The non-degummed sheets show lower UTS_{sheet} but a smaller standard deviation when compared to the degummed sheets. There are statistically significant differences in UTS at the 1 mm/min strain rate between the non-degummed and degummed sheets, however the 10 mm/min UTS_{sheet} are not significantly different. The results from the two-way ANOVA show that the degumming process has a larger statistically significant effect (p = 0.0002) on UTS_{sheet} than the strain rates (p= 0.0387). The maximum strain ($\varepsilon_{max,sheet}$, Fig. 4**D**) of the sheets does not have as significant differences between strain rate or the degumming process. Since all the sheets rip or fracture at strain rates outside of their linear, elastic region, the degummed sheets show more variability in their plastic regions at high strains. The two-way ANOVA results show that the degumming processing (p = 0.005) has a statistically significant impact on $\varepsilon_{max,sheet}$ but that the strain rate does not (p= 0.7843). Overall, degumming has the most significant impact on the E_{sheet}, UTS_{sheet}, and $\varepsilon_{max,sheet}$ of *P. interpunctella* sheets.

Upon degumming, a decrease in the elastic response of the sheets is expected due to the increase in β-sheet content, as shown in Fig. 2**K** (blue vs. purple, 45 % vs. 48 %, respectively) and the removal of the outer coating from the surface of the fibers. Exposure to water and high temperatures during degumming can promote rearrangement of the inter- and intramolecular hydrogen bond networks within silk proteins, generating new crystalline structures and a reorganization of protein secondary structures.[77,84] This shift in secondary structure may modify the mechanisms by which the fibers respond to stress (extension) and correlate to increased mechanical strength and stiffness in degummed materials. Degummed sheets were found to produce larger Young's modulus (20–44 MPa, Fig. 4**B**) and UTS (8–18 MPa, Fig. 4**C**) with a more plastic and brittle response to static strain. The high variability in standard deviations is attributed to the random alignment of fibers in the material and the general variability in natural materials, especially silks [52]. This work successfully built upon previous mechanical property evaluation of non-degummed sheets [23] and represents a more reproducible data set from improved methodology of loading samples for DMA.

3.3.2. Bulk mechanical properties of *P. interpunctella* aligned silk fiber bundles

For the purposes of bulk mechanical testing, aligned fiber bundles are more relevant to handle, measure, and compare to other fibers used in biomedical and environmental applications, such as those described in Table 1. Degumming methods for the sheets were effective for the aligned bundled *P. interpunctella* fibers, as visualized through comparison of SEM micrographs (Fig. 5**AB**). The non-degummed aligned fiber bundles are hypothesized to have a more viscoelastic response, whereas the degummed aligned fiber bundles will have a higher Young's modulus and UTS, with a more plastic-like mechanical response. The expected shifts in mechanics and behavior at higher strain rates are attributed to both changes in protein composition (loss of fiber coating) and the hypothesis that degumming alters protein-protein interactions and increases β-sheet content (FTIR spectral data in Fig. 2**J**).

Following a similar extensional testing protocol to what was used for the *P. interpunctella* sheets, Fig. 5**C** shows stress-strain curves from tensile testing of non-degummed (blue) and degummed (purple) *P. interpunctella* aligned fiber bundles at two different strain rates, which can be seen in **Supplemental Video 2.** Each stress-strain curve was analyzed to determine Young's modulus (E_{bundle}, MPa), UTS (MPa), and the maximum strain ($\varepsilon_{max,bundle}$) (Supplemental Fig. S6B) and the averages are reported in Supplemental Table 1. Fig. 5**D** depicts significant differences between E_{bundle} of the non-degummed (536 ± 127 MPa, 10 mm/mm) versus degummed (3052 ± 965 MPa, 10 mm/mm) fiber bundles at both strain rates, showing a 5.7-fold change in MPa as a result of degumming. While there do exist differences when comparing strain rates, these overall parameters are not statistically significant, demonstrating that the aligned fiber bundles are less dependent on strain rate compared to the random sheets. The results from the two-way ANOVA statistical analysis showed that the effect of strain rate on Young's modulus (E_{bundle}) was not significant (p = 0.066), while the effect of degumming was highly statistically significant (p< 0.0001). Similar trends exist for the UTS_{bundle} and $\varepsilon_{max,bundle}$ results (Fig. 5**E,F**). From a two-way ANOVA analysis, the effect on UTS_{bundle} from strain rate is insignificant (p = 0.1582), while the effect from degumming is statistically significant (p< 0.0001). Similarly, two-way ANOVA statistical analysis shows that the interaction between strain rate and degumming

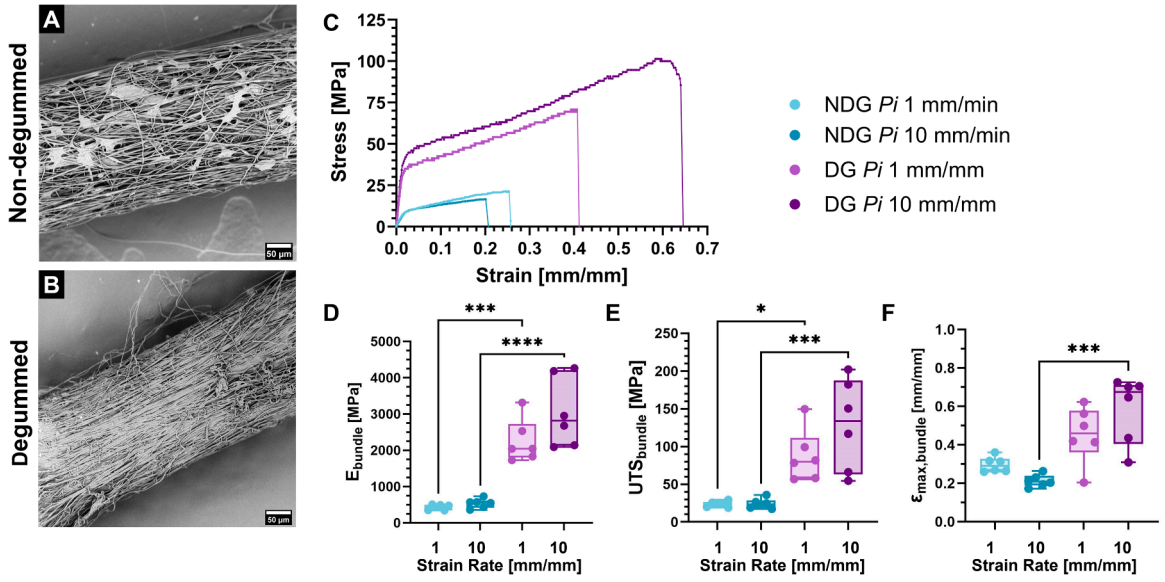

Fig. 5. Static tensile testing of *P. interpunctella* (*Pi*) aligned fiber bundles. (**A**) SEM image of a non-degummed (NDG) *P. interpunctella* fiber bundle. (**B**) SEM image of a degummed (DG) *P. interpunctella* fiber bundle. (**C-F**) Static tensile testing of *P. interpunctella* fiber bundles at 1 mm/min (lighter color points) and 10 mm/min (darker color points) strain rates. (**C**) Representative stress-strain curves for non-degummed (NDG, blue) and degummed (DG, purple) fiber bundles. (**D**) Young's modulus (E_{bundle}, n = 6) (**E**) Ultimate tensile strength (UTS_{bundle}, n = 6) and (F) strain at max elongation ($\varepsilon_{max,bundle}$, n = 6). Data are expressed as mean ± standard deviation. Analyzed with 2-Way ANOVA with Tukey's test post-hoc analysis. Statistical significance is reported as *p < 0.05, ***p < 0.001, and ****p < 0.0001.

have some statistically significant ($p = 0.033$) effect on $\varepsilon_{max,bundle}$, but that the impact of strain rate ($p = 0.6084$) itself is not statistically significant, while the effect of degumming ($p < 0.0001$) on $\varepsilon_{max,bundle}$ is highly significant.

Overall, degumming has the most significant impact on the extensional properties of *P. interpunctella* aligned fiber bundles across all parameters investigated. These differences are hypothesized to result from altering the protein composition and protein-protein interactions (observed in secondary structure differences, Fig. 2**K**) of the fiber. Together, these data suggest that mechanical properties are not a function of fiber diameter or just the amount of protein present, but in these semi-crystalline materials, protein composition and protein secondary structures greatly impact bulk mechanical properties.

3.3.3. Microscale mechanical and adhesive properties of *P. interpunctella* silk fibers

Atomic force microscopy (AFM) was performed on individual fibers from non-degummed and degummed *P. interpunctella* sheets to assess microscale mechanical and adhesive properties and resulting data are shown in Fig. 6. Force curves of the approach to the fiber surface and retraction from the surface were obtained at each pixel in the force maps and used to calculate the Young's modulus (E_{fiber}) and adhesive force at each point (Supplemental Fig. S9A). Representative distribution maps of E_{AFM} and adhesion force for non-degummed *P. interpunctella* fibers are shown in Fig. 6**B and C**, respectively. Raw data and examples of the numeric distribution of these parameters are shown in Supplemental Fig. S9B and **C**. The same analysis was performed on degummed *P. interpunctella* fibers, with representative distribution maps of Young's modulus and adhesion shown in Fig. 6**E and F**.

The overall trends in Young's modulus observed in the bulk mechanical assessment (E_{sheet}: Fig. 4**B**; E_{bundle}: Fig. 5**D**) of *P. interpunctella* sheets and aligned fiber bundles are also seen in microscale assessments of individual fibers. Non-degummed fibers (blue) exhibit a lower E_{fiber} compared to degummed fibers (purple, Fig. 6**G**), another indication that the removal of the silk fiber coating and an increase in β-sheet content results in a less elastic response ($p < 0.001$). Comparisons to non-degummed *B. mori* silk fibers (Supplemental Fig. S11) highlight the importance of protein sequence in measured mechanical properties, with the *B. mori* silk fibers exhibiting similar trends to comparisons made to *B. mori* literature,[12–14,19,23] where the fiber modulus (E) and tensile strength (UTS) are greater for *B. mori* silk fibers compared to *P. interpunctella* silk fibers. These differences are hypothesized to result from changes in protein sequences and the presence (or absence) of supplemental proteins in the silk fiber as a result of any differences in silk fiber spinning within *P. interpunctella* vs. *B. mori*.

To further characterize the differences between a degummed fiber and a non-degummed fiber, changes in adhesivity on the fiber surface were investigated. Degummed fibers are expected to exhibit a decrease in the adhesive forces due to the removal of the sticky, outer fiber coating, which contains sericins and other key proteins that improve the silk fiber function for the insect in nature. This hypothesis holds, as the degummed fibers had lower adhesive forces when compared to non-degummed fibers (Fig. 6**H**). *B. mori* fibers displayed a much larger spread of adhesive forces, attributed to limited representation of the entire fiber through the small window of analysis used with the AFM assessments (see supplemental discussion in **Supplemental Section 5.1**); however, it does show that non-degummed *B. mori* fibers, on average, have higher adhesion forces than both non-degummed and degummed *P. interpunctella* fibers (Supplemental Fig. S11F). While understandings of *P. interpunctella* sericin proteins and sericin fiber coating is not yet fully described in literature, a potential hypothesis can be derived from the results from Fig. 2**I**. Removal of the outer sericin coating resulted in a lower % decrease in *P. interpunctella* fiber diameter when compared to *B. mori*, pointing to a difference in amount of fiber coating proteins removed or differences in the initial thickness of the sericin coating. It is possible that the contrast of adhesive properties could result from this difference in the thickness of the coating in addition to potential dissimilarities of properties, composition and utility of the individual coating proteins. Further investigations into the role of silk fibers and their structure and function from a biological context will improve understandings of the cause for these measured changes in mechanics.

3.3.4. Perspectives on the role of *P. interpunctella* silk fiber thermal and mechanical properties toward future applications

The broad application space of synthetic and natural fibers is due to the range of properties achievable, as certain characteristics (i.e., more crystalline, more elastic, higher stability) are beneficial in differing applications [18,38,45,85]. In this manuscript, these defined properties were determined for *P. interpunctella* silk fibers, in addition to

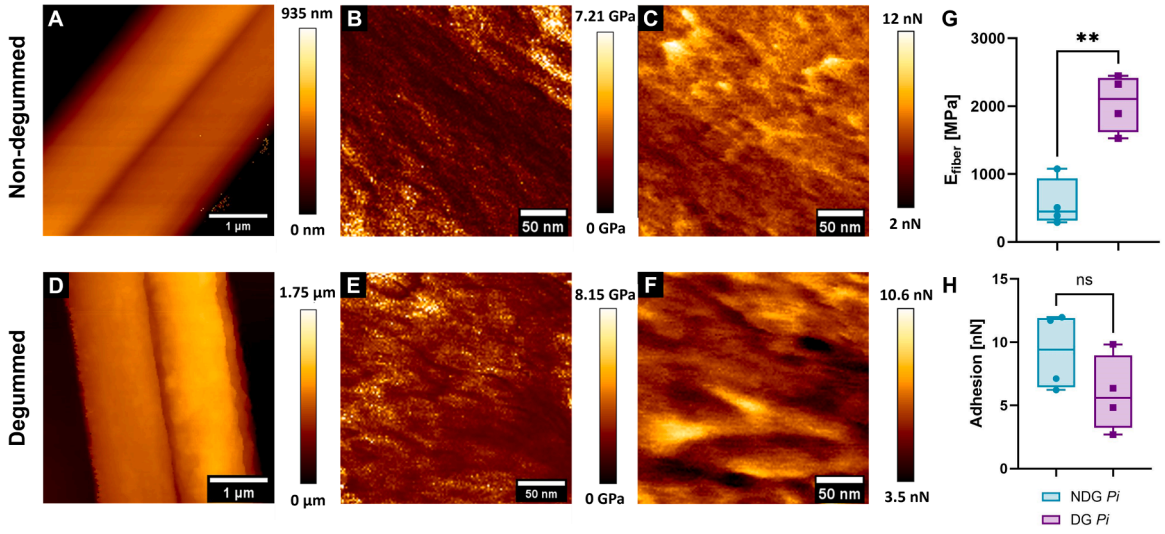

Fig. 6. Atomic force microscopy (AFM) of *P. interpunctella* (*Pi*) fibers. Representative height topography images for non-degummed (NDG) (**A**) and degummed (DG) (**D**) silk fibers. Force spectroscopy was completed on 500 nm regions on single fibers. Representative distribution maps of Young's modulus for non-degummed (**B**) and degummed (**E**) fibers. Representative distribution maps of adhesive forces for non-degummed (**C**) and degummed (**F**) fibers. Distributions of height, Young's modulus (E_{fiber}), and adhesion forces are depicted by the color scale accompanying the image. (**G**) Young's modulus and (**H**) adhesion (n = 4). Data are expressed as mean ± standard deviation. Analyzed with unpaired parametric *t*-test. Statistical significance is reported as $^{**}p < 0.001$.

assessments of crystallinity and behavior at the microscale to provide a more comprehensive understanding of function as a raw material and to identify its potential towards biomaterial research. Continuity was found across all three levels of mechanical assessments, accounting for expected sample heterogeneity [52]. In Table 1, the thermal and mechanical properties are summarized for common synthetic and natural fibers used or proposed for biomaterial research, specifically focusing on the T_g, T_m, tensile modulus, and tensile strength. However, it is important to acknowledge that these parameters can be highly dependent on sample size, experimental conditions, methodology (*e.g.,* temperature, rate), and instruments. In this work, experimental parameters that are commonly used in existing literature (e.g., TGA ramp rate: 10 C/min, DMA strain rate: 1 and 10 mm/min) [86] were used to contextualize *P. interpunctella* in the space of synthetic and natural fibers.

3.3.5. *Perspectives on Young's modulus and ultimate tensile strength*

The extensional mechanical properties of tensile (Young's) modulus and tensile strength (UTS) for relevant synthetic and natural fibers in literature are compared to average experimental properties for *P. interpunctella* aligned fiber bundles (Fig. 7). When compared to other silk fibers, *P. interpunctella* has significantly lower tensile modulus (E) and strength (UTS). Non-degummed *P. interpunctella* fiber bundles are at least an order of magnitude lower in tensile modulus and strength values than that of *B. mori*, the gold standard in the silk field. While degumming increases the magnitude of the tensile modulus and tensile strength in *P. interpunctella*, reported mechanical properties are still around 3-times lower than the other silk types reported. These differences are likely due to the secondary structure of *P. interpunctella* silk. The lower β-sheet content (Fig. 2**K**) and less repetitive structure were expected to produce more elastic and responsive materials rather than higher strength as seen in some silks (*e.g., G. mellonella, A. pernyi,* and *A. assamensis*) and even *B. mori* to some extent [12,19,37]. The experimental mechanical properties reported for the *P. interpunctella* fiber bundles align more closely with reported mechanical properties of traditional polymer fibers, rather than other silk derived fibers.

While *P. interpunctella* differs from other native silk fibers, the degummed *P. interpunctella* silk has and equivalent range in tensile modulus (2 – 4 GPa) and tensile strength (50 – 100 MPa) which has potential as a replacement to synthetic polymer sources (Table 1). Degummed *P. interpunctella* silk fibers are specifically similar to synthetic polymers such as Nylon 6 [1–3] and Polyethylene terephthalate (PET) [5] (Fig. 7), which are commonly used in advanced manufacturing [2] and packaging [5]. Nylon 6 is reported to be a flexible and elastic fiber [2], with similar mechanical and thermal characteristics as

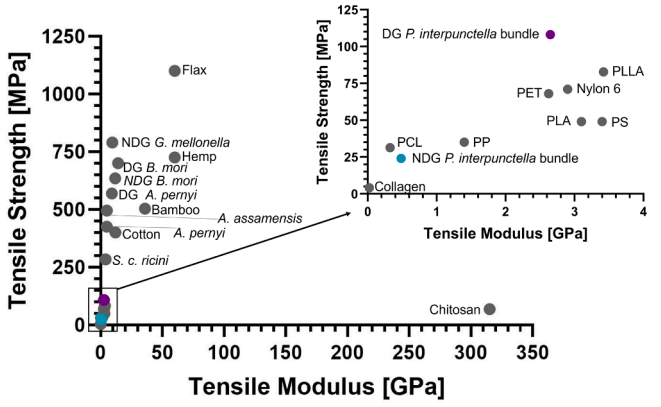

Fig. 7. Bulk extensional average tensile strength versus average tensile modulus of various natural and synthetic fibers (gray circles) found in literature (Table 1). DMA experimental average bulk properties for non-degummed (NDG) *P. interpunctella* aligned fiber bundles (blue) and degummed (DG) *P. interpunctella* aligned fiber bundles (purple) are shown for comparison to currently available materials.

degummed *P. interpunctella* fibers. Nylon has slow degradation rates due to its high levels of crystallinity [87], and, as future work explores *P. interpunctella* degradation, it is hypothesized from previous silk literature that *P. interpunctella* may degrade more quickly due to its lower crystallinity levels [41,43], providing a natural, protein alternative that matches the mechanical and thermal properties of Nylon fibers. Non-degummed *P. interpunctella* silk fibers are more similar in mechanical properties to synthetic fibers such as polypropylene (PP) and polycaprolactone (PCL). The tensile modulus (0.5 – 1.5 GPa) and tensile strength (20 – 30 MPa) (Table 1) in this range has many applications in biomaterials and medicine [88–91]. *P. interpunctella* silk may be an advantageous replacement or supplement to these synthetic fibers due to its naturally derived and renewable source, allowing for greater control over material degradation rates *in vivo* and providing non-toxic by-products (amino acids) [41].

Shirk *et al.* previously demonstrated that non-degummed *P. interpunctella* silk sheets had mechanical properties that aligned closely with soft tissues such as cartilage [23]. Similar properties are reported in this work, with degummed *P. interpunctella* sheets having slightly higher mechanical strength over the various strain rates. However, for biological applications, aligned structures are more commonly found in the body, thus the aligned fiber bundles may be a more relevant material type than randomly organized sheets. *P. interpunctella* aligned fiber bundles closely match the mechanical properties of highly aligned tissue types such as tendon and ligaments [92]. PCL and polylactic acid (PLA) fibers generated through a variety of methods such as electrospinning have utility in aligned soft tissue applications such as tendon and ligament engineering [93]. Degummed and non-degummed *P. interpunctella* fibers fall within the range of tensile strength and modulus of current materials demonstrating that it may be an alternative material for tendon regeneration applications. The structure of aligned *P. interpunctella* fiber bundles also match the structural hierarchy of the native collagen subunits found in tendon and the stress-strain curves of *P. interpunctella* aligned fiber bundles match fracture points found in the plastic regime of native tissue [93]. However, to even suggest that these applications are possible, the biocompatibility of these materials and their impact on cell growth and metabolism must be understood.

3.4. *Cell-material interactions of P. interpunctella silk sheets*

To understand the potential for these materials to have applications in a biomedical context, preliminary cytotoxicity experiments were performed. Adhesion and proliferation on raw and degummed silk fibers is not an ideal way to use this material as most silk fibroin-based biomaterials are generated from regenerated silk fibroin solutions that are then used as a polymer solution to form new materials. Moreover, the bioactivity of silk fibers and silk-based materials varies across species due to varying chemical composition and surface structures that influence cell-material interactions. The most commonly used silk fibroin source, *B. mori*, lacks amino acid sequences known to support cell attachment, and instead engages with cells though physical adhesion of cell binding molecules [94], such as serums or other extracellular matrix proteins. When processed appropriately, silk fibroins from *B. mori* have shown limited unwanted immune responses, behaving as an inert material rather than a toxic one, with minimal to no fibrotic capsule formation upon implantation [95–99]. While these types of investigations are necessary to fully understand the potential for *P. interpunctella* silk as a biomaterial for cell growth and regeneration, this initial investigation serves to understand if these further investigations are warranted. To ask these initial questions, sterile degummed and non-degummed *P. interpunctella* silk sheets were prepared. While it is expected that the autoclaving process used to sterilize the material will adjust the protein secondary structure and mechanical properties outside of what is presented in this manuscript, this preparation is necessary to fully investigate attachment, proliferation, and adhesion.

To assess the validity of further investigation of laboratory reared *P. interpunctella* silk, normal human lung fibroblasts (NHLF) were seeded onto autoclaved silk fiber sheets pre- and post- degumming using serum containing and serum free cell culture media formulations, as it is well known that large serum proteins physisorb to the surface of most protein-based materials, including silk fibroin. This physisorption aids in initial cell attachment. In all conditions, fibroblasts were able to adhere to the *P. interpunctella* silk sheets and relative metabolic activity remained constant over 3 days in culture, even in the absence of fetal bovine serum (FBS) as shown in Fig. 8. These results align with previous investigations of *P. interpunctella* silk, wherein human fetal lung fibroblasts (MRC-5) were successfully cultured on *P. interpunctella* silk sheets for 72 hours, finding that cells were strongly adhered to the silk surface [67]. Cells display normal fibroblast morphology on Day 1 (Fig. 8**A,C**). After 3 days, cell morphology on the non-degummed *P. interpunctella* sheets shows the presence of punctate actin staining, suggesting some cell death or shift in phenotype Fig. 8**B vs. D**. Across all conditions, metabolic activity remained constant when normalized to the respective tissue culture plastic condition (Supplemental Fig. S12), suggesting no change in growth rate over time. The addition of FBS did not significantly impact metabolic activity for both non-degummed ($p = 0.2841$) and degummed ($p = 0.1458$) silk sheets (Supplemental Fig. S13). Two-way ANOVA analysis determined no significance on time ($p = 0.6132$) or degumming ($p = 0.8761$) on metabolic activity of NHLF cultured without FBS. Overall, these results suggest that for sterilized degummed and raw silk materials, there does not exist any active epitopes that promote fibroblast cell death and thus continued investigation and future work utilizing these materials for biomedical applications is warranted.

4. Conclusions

Silk materials have a wide range of applications from advanced manufacturing to biotechnology. As the use of these materials moves from a research space to a commercial venture, additional polymers with different properties will be useful to create impactful products. Prior work developed indoor rearing protocols with tight control over environmental parameters, providing a consistent alternative source of silk fibroin. To capitalize on the potential of these *P. interpunctella* silk materials, the thermal and mechanical properties of the silk fibers were fully characterized, providing insight on the sequence-structure-function relationships that drive material performance. Specifically, sequence-structure relationships are explored using spectral and microscopy techniques, focusing on amino acid sequence and secondary structure contributions. Structure-function relationships are explored through the connections between spectral, thermal, and mechanical data, reflecting on the role of degumming, or fiber coating removal (Fig. 1), in resulting material properties. Confirmation of *P. interpunctella* silk degumming was explored, and both raw and degummed *P. interpunctella* fibers were observed to be semi-crystalline materials with high β-sheet content, similar to *B. mori*, despite having substantially different amino acid sequences that are responsible for these crystalline structures. These crystalline domains contribute to mechanical properties, where *P. interpunctella* silk materials exhibit viscoelastic properties at low strain rates. However, the organization of these domains may also contribute to the brittle fracture of the materials at higher strains and resulting ultimate tensile strength (UTS) as observed in **Supplemental Video 1** (sheet) and **2** (bundle).

Results show that *P. interpunctella* silk fibers are similar to polypropylene and poly-lactic acid fibers [1] and degummed *P. interpunctella* silk fibers are similar to Nylon, PET, or PLLA fibers [1–5] in terms of mechanical strength and modulus (Fig. 7). For example, comparisons showed that resulting mechanical and thermal properties ($T_m = 250$ ℃, Fig. 3) of *P. interpunctella* silk fibers align closely with reported mechanical and thermal properties of Nylon (Fig. 7, Table 1), a highly crystalline synthetic polymer fiber with limited potential for environmental degradation. The use of silk materials, such as *P. interpunctella* fibers, as a natural, biodegradable alternative can help address environmental concerns while maintaining material performance. Preliminary investigations herein with normal human lung fibroblasts agree with prior literature [66,67] that these materials are worth pursuing for biomedical applications. Taken together, these results warrant continued investigation into the regeneration of these silk fibers and production of silk fibroin solutions to continue efforts toward the production of *P. interpunctella* silk materials, such as nanoparticles, films, and sponges.

CRediT authorship contribution statement

Lauren E Eccles: Writing – review & editing, Writing – original draft, Visualization, Validation, Project administration, Methodology, Investigation, Formal analysis, Data curation, Conceptualization.

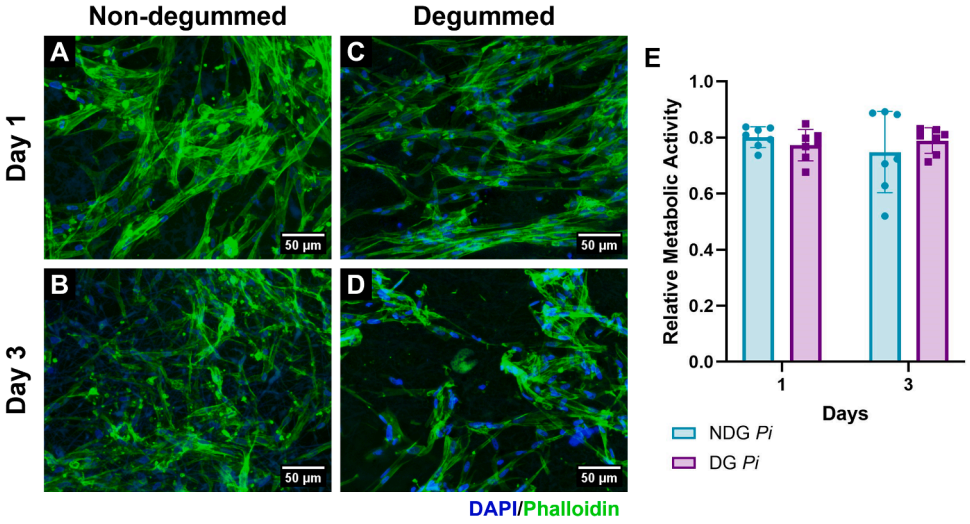

Fig. 8. Cell adhesion and growth on *P. interpunctella* silk sheets without FBS supplementation. Representative fluorescent image of NHLF cultured on non-degummed (NDG) *P. interpunctella* silk sheets for 1 (A) and 3 (B) days stained with DAPI (blue) and phalloidin (green). Representative fluorescent image of NHLF cultured on degummed (DG) *P. interpunctella* silk sheets for 1 (C) and 3 (D) stained with DAPI and phalloidin. (E) Metabolic activity of NHLF cells cultured on non-degummed (blue) and degummed (purple) silk sheets at 1 and 3 days. Data is normalized to metabolic activity of cells on tissue culture plastic and shown as mean ± standard deviation (n = 7).

Whitney L. Stoppel: Writing – review & editing, Writing – original draft, Visualization, Validation, Supervision, Resources, Project administration, Funding acquisition, Data curation, Conceptualization. **Jasmine B McTyer:** Writing – review & editing, Writing – original draft, Visualization, Methodology, Investigation, Formal analysis. **Elizabeth L Aikman:** Writing – review & editing, Writing – original draft, Visualization, Validation, Methodology, Investigation, Formal analysis. **Adelyn L Richgels:** Writing – review & editing, Visualization. **Isabel L Matías Cruz:** Writing – review & editing, Visualization.

Declaration of Competing Interest

The authors declare the following financial interests/personal relationships which may be considered as potential competing interests: Whitney Stoppel reports financial support was provided by National Institutes of Health. Whitney L Stoppel reports a relationship with National Institutes of Health that includes: funding grants. Whitney Stoppel reports a relationship with National Science Foundation that includes: funding grants. Elizabeth Aikman reports a relationship with National Science Foundation that includes: funding grants. If there are other authors, they declare that they have no known competing financial interests or personal relationships that could have appeared to influence the work reported in this paper.

Acknowledgements

The Stoppel Research Group would like to thank undergraduates in the laboratory, including Andrea Orozcotorres, Rebecca Liwang, and Zachary Ostrander, for maintenance of insect cultures and silk collection. All Stoppel Lab members would like to acknowledge support from the National Institutes of Health National Institute of General Medical Sciences Maximizing Investigators' Research Award (NIH NIGMS R35-GM147041) and an Integrative Biology Award from the National Science Foundation (NSF MCB-2217159). All Stoppel Lab members acknowledge support from the William P and Tracy Cirioli Professorship at the University of Florida. ELA acknowledges support from the National Science Foundation Graduate Research Fellowship (DGE-2236414). Any opinions, findings, and conclusions or recommendations expressed in this manuscript are those of the authors and do not necessarily reflect the views of the National Science Foundation or the National Institutes of Health. Equipment at the Research Service Centers of the Herbert Wertheim College of Engineering at the University of Florida were utilized with extremely valuable assistance from Gary Scheiffele, Ph.D. All authors would like to acknowledge support from the University of Florida and the University of Florida Herbert Wertheim College of Engineering and Department of Chemical Engineering.

Supporting Information

Supplemental information is provided in a supplemental file. Raw data will be provided upon request or can be accessed through this link.

Appendix A. Supporting information

Supplementary data associated with this article can be found in the online version at doi:10.1016/j.mtcomm.2024.111416.

Data Availability

The supplement and main document contain a link to the raw data.

References

[1] L. Ranakoti, B. Gangil, S.K. Mishra, T. Singh, S. Sharma, R.A. Ilyas, S. El-Khatib, Critical review on polylactic acid: properties, structure, processing, biocomposites, and nanocomposites, Materials (Basel) 15 (12) (2022) 4312.
[2] I.P. Beckman, C. Lozano, E. Freeman, G. Riveros, Fiber selection for reinforced additive manufacturing, Polymers (Basel) 13 (14) (2021) 2231.
[3] J.P. Greene, Microstructures of polymers, Automot. Plast. Compos. (2021) 27–37.
[4] S. Farah, D.G. Anderson, R. Langer, Physical and mechanical properties of PLA, and their functions in widespread applications - a comprehensive review, Adv. Drug Deliv. Rev. 107 (2016) 367–392.
[5] R. Panowicz, M. Konarzewski, T. Durejko, M. Szala, M. Lazinska, M. Czerwinska, P. Prasula, Properties of polyethylene terephthalate (PET) after thermo-oxidative aging, Materials (Basel) 14 (14) (2021) 3833.
[6] S. Vigneshwaran, R. Sundarakannan, K.M. John, R.D.J. Johnson, K.A. Prasath, S. Ajith, V. Arumugaprabu, M. Uthayakumar, Recent advancement in the natural fiber polymer composites: a comprehensive review, J. Clean. Prod. 277 (2020) 124109.
[7] I. Yamaguchi, S. Itoh, M. Suzuki, M. Sakane, A. Osaka, J. Tanaka, The chitosan prepared from crab tendon I: the characterization and the mechanical properties, Biomaterials 24 (12) (2003) 2031–2036.
[8] R.A. Ilyas, H.A. Aisyah, A.H. Nordin, N. Ngadi, M.Y.M. Zuhri, M.R.M. Asyraf, S. M. Sapuan, E.S. Zainudin, S. Sharma, H. Abral, M. Asrofi, E. Syafri, N.H. Sari, M. Rafidah, S.Z.S. Zakaria, M.R. Razman, N.A. Majid, Z. Ramli, A. Azmi, S. P. Bangar, R. Ibrahim, Natural-fiber-reinforced chitosan, chitosan blends and their nanocomposites for various advanced applications, Polymers (Basel) 14 (5) (2022) 874.
[9] G.D. Pins, D.L. Christiansen, R. Patel, F.H. Silver, Self-assembly of collagen fibers. Influence of fibrillar alignment and decorin on mechanical properties, Biophys. J. 73 (4) (1997) 2164–2172.
[10] G. Arpitha, B. Yogesha, An overview on mechanical property evaluation of natural fiber reinforced polymers, Mater. Today.: Proc. 4 (2) (2017) 2755–2760.
[11] R. Moriana, F. Vilaplana, S. Karlsson, A. Ribes, Correlation of chemical, structural and thermal properties of natural fibres for their sustainable exploitation, Carbohydr. Polym. 112 (2014) 422–431.
[12] C. Guo, J. Zhang, J.S. Jordan, X. Wang, R.W. Henning, J.L. Yarger, Structural comparison of various silkworm silks: an insight into the structure-property relationship, Biomacromolecules 19 (3) (2018) 906–917.
[13] S. Mazzi, E. Zulker, J. Buchicchio, B. Anderson, X. Hu, Comparative thermal analysis of Eri, Mori, Muga, and Tussar silk cocoons and fibroin fibers, J. Therm. Anal. Calor. 116 (3) (2014) 1337–1343.
[14] R.O. Moreno-Tortolero, Y. Luo, F. Parmeggiani, N. Skaer, R. Walker, L.C. Serpell, C. Holland, S.A. Davis, Molecular organization of fibroin heavy chain and mechanism of fibre formation in Bombyx mori, Commun. Biol. 7 (1) (2024) 786.
[15] X. Hu, D. Kaplan, P. Cebe, Determining beta-sheet crystallinity in fibrous proteins by thermal analysis and infrared spectroscopy, Macromolecules 39 (18) (2006) 6161–6170.
[16] I. Elfaleh, F. Abbassi, M. Habibi, F. Ahmad, M. Guedri, M. Nasri, C. Garnier, A comprehensive review of natural fibers and their composites: an eco-friendly alternative to conventional materials, Results Eng. 19 (2023) 101271.
[17] S.F. Hamad, N. Stehling, C. Holland, J. Foreman, C. Rodenburg, Low-Voltage SEM of natural plant fibers: microstructure properties (surface and cross-section) and their link to the tensile properties, Procedia Eng. 200 (2017) 295–302.
[18] C. Vepari, D.L. Kaplan, Silk as a Biomaterial, Prog. Polym. Sci. 32 (8-9) (2007) 991–1007.
[19] L. Cheng, J. Shao, F. Wang, Z. Li, F. Dai, Strain rate dependent mechanical behavior of B. mori silk, A. assama silk, A. pernyi silk and A. ventricosus spider silk, Mater. Des. 195 (2020) 108988.
[20] F. Sehnal, T. Sutherland, Silks produced by insect labial glands, Prion 2 (4) (2008) 145–153.
[21] A.D. Malay, R. Sato, K. Yazawa, H. Watanabe, N. Ifuku, H. Masunaga, T. Hikima, J. Guan, B.B. Mandal, S. Damrongsakkul, K. Numata, Relationships between physical properties and sequence in silkworm silks, Sci. Rep. 6 (2016) 27573.
[22] C. Offord, F. Vollrath, C. Holland, Environmental effects on the construction and physical properties of Bombyx mori cocoons, J. Mater. Sci. 51 (24) (2016) 10863–10872.
[23] B.D. Shirk, I.Torres Pereira Meriade Duarte, J.B. McTyer, L.E. Eccles, A.H. Lateef, P.D. Shirk, W.L. Stoppel, Harvesting silk fibers from plodia interpunctella: role of environmental rearing conditions in fiber production and properties, ACS Biomater. Sci. Eng. 10 (4) (2024) 2088–2099.
[24] T.V. Barve, R.K. Godfrey, C.G. Storer, A.Y. Kawahara, Larval and pupal silk variation in the indian meal moth (Plodia interpunctella): the impact of overcrowding and temperature, J. Lepid. ' Soc. 77 (2) (2023) 116–121, 6.
[25] C. Hopfe, B. Ospina-Jara, T. Schulze, M. Tischer, D. Morales, V. Reinhartz, R. E. Esfahani, C. Valderrama, J. Perez-Rigueiro, C. Bleidorn, H. Feldhaar, J. Cabra-Garcia, T. Scheibel, Impact of environmental factors on spider silk properties, Curr. Biol.: CB 34 (1) (2024) 56–67, e5.
[26] X. Hu, D. Kaplan, P. Cebe, Dynamic protein-water relationships during β-sheet formation, Macromolecules 41 (11) (2008) 3939–3948.
[27] Q. Lu, H. Zhu, C. Zhang, F. Zhang, B. Zhang, D.L. Kaplan, Silk self-assembly mechanisms and control from thermodynamics to kinetics, Biomacromolecules 13 (3) (2012) 826–832.
[28] C. Holland, A.E. Terry, D. Porter, F. Vollrath, Comparing the rheology of native spider and silkworm spinning dope, Nat. Mater. 5 (11) (2006) 870–874.
[29] A. Koeppel, C. Holland, Progress and trends in artificial silk spinning: a systematic review, ACS Biomater. Sci. Eng. 3 (3) (2017) 226–237.
[30] A. Koeppel, N. Stehling, C. Rodenburg, C. Holland, Spinning beta silks requires both ph activation and extensional stress, Adv. Funct. Mater. 31 (30) (2021) 2103295.

[31] P.R. Laity, E. Baldwin, C. Holland, Changes in silk feedstock rheology during cocoon construction: the role of calcium and potassium ions, Macromol. Biosci. 19 (3) (2019) e1800188.
[32] C. Schaefer, P.R. Laity, C. Holland, T.C.B. McLeish, Silk protein solution: a natural example of sticky reptation, Macromolecules 53 (7) (2020) 2669–2676.
[33] J. Sparkes, C. Holland, The energy requirements for flow-induced solidification of silk, Macromol. Biosci. 19 (3) (2019) e1800229.
[34] C. Dicko, J.M. Kenney, D. Knight, F. Vollrath, Transition to a beta-sheet-rich structure in spidroin in vitro: the effects of pH and cations, Biochemistry 43 (44) (2004) 14080–14087.
[35] C. Dicko, D. Knight, J.M. Kenney, F. Vollrath, Secondary structures and conformational changes in flagelliform, cylindrical, major, and minor ampullate silk proteins. Temperature and concentration effects, Biomacromolecules 5 (6) (2004) 2105–2115.
[36] I. Greving, A.E. Terry, C. Holland, M. Boulet-Audet, I. Grillo, F. Vollrath, C. Dicko, Structural diversity of native major ampullate, minor ampullate, cylindriform, and flagelliform silk proteins in solution, Biomacromolecules 21 (8) (2020) 3387–3393.
[37] M.J. Glasper, Collection, Processing, and Characterization of Galleria mellonella Silk, Department of Human Ecology, University of Alberta, Alberta, Canada, 2019.
[38] G.H. Altman, F. Diaz, C. Jakuba, T. Calabro, R.L. Horan, J. Chen, H. Lu, J. Richmond, D.L. Kaplan, Silk-based biomaterials, Biomaterials 24 (3) (2003) 401–416.
[39] M.S. Zafar, D.J. Belton, B. Hanby, D.L. Kaplan, C.C. Perry, Functional material features of Bombyx mori silk light versus heavy chain proteins, Biomacromolecules 16 (2) (2015) 606–614.
[40] E.L. Aikman, A.P. Rao, Y. Jia, E.E. Fussell, K.E. Trumbull, J. Sampath, W.L. Stoppel, Impact of crystalline domains on long-term stability and mechanical performance of anisotropic silk fibroin sponges, J. Biomed. Mater. Res A 112 (9) (2024) 1451–1471.
[41] J.F. Jameson, M.O. Pacheco, J.E. Butler, W.L. Stoppel, Estimating kinetic rate parameters for enzymatic degradation of lyophilized silk fibroin sponges, Front Bioeng. Biotech. 9 (537) (2021) 664306.
[42] B.P. Partlow, A.P. Tabatabai, G.G. Leisk, P. Cebe, D.L. Blair, D.L. Kaplan, Silk fibroin degradation related to rheological and mechanical properties, Macromol. Biosci. 16 (5) (2016) 666–675.
[43] Q. Lu, B. Zhang, M. Li, B. Zuo, D.L. Kaplan, Y. Huang, H. Zhu, Degradation mechanism and control of silk fibroin, Biomacromolecules 12 (4) (2011) 1080–1086.
[44] M.O. Pacheco, H.M. Lutz, J. Armada, N. Davies, I.K. Gerzenshtein, A.S. Cakley, B. D. Spiess, W.L. Stoppel, Silk fibroin particles as carriers in the development of hemoglobin-based oxygen carriers, Adv. Nanobiomed Res 3 (9) (2023) 2300019.
[45] D.N. Rockwood, R.C. Preda, T. Yucel, X. Wang, M.L. Lovett, D.L. Kaplan, Materials fabrication from Bombyx mori silk fibroin, Nat. Protoc. 6 (10) (2011) 1612–1631.
[46] Y. Chen, W. Yang, W. Wang, M. Zhang, M. Li, Bombyx mori silk fibroin scaffolds with Antheraea pernyi Silk fibroin micro/nano fibers for promoting EA. hy926 cell proliferation, Materials (Basel) 10 (10) (2017) 1153.
[47] J.K. Sahoo, O. Hasturk, T. Falcucci, D.L. Kaplan, Silk chemistry and biomedical material designs, Nat. Rev. Chem. 7 (5) (2023) 302–318.
[48] B.P. Partlow, C.W. Hanna, J. Rnjak-Kovacina, J.E. Moreau, M.B. Applegate, K. A. Burke, B. Marelli, A.N. Mitropoulos, F.G. Omenetto, D.L. Kaplan, Highly tunable elastomeric silk biomaterials, Adv. Funct. Mater. 24 (29) (2014) 4615–4624.
[49] B.D. Shirk, D.L. Heichel, L.E. Eccles, L.I. Rodgers, A.H. Lateef, K.A. Burke, W. L. Stoppel, Modifying naturally occurring, nonmammalian-sourced biopolymers for biomedical applications, ACS Biomater. Sci. Eng. 10 (10) (2024) 5915–5938.
[50] S.A.L. Matthew, F.P. Seib, Silk bioconjugates: from chemistry and concept to application, ACS Biomater. Sci. Eng. 10 (1) (2024) 12–28.
[51] H.R. Liu, Z.Y. Sun, C.C. Guo, Chemical modification of silk proteins: current status and future prospects, Adv. Fiber Mater. 4 (4) (2022) 705–719.
[52] G. Greco, H. Mirbaha, B. Schmuck, A. Rising, N.M. Pugno, Artificial and natural silk materials have high mechanical property variability regardless of sample size, Sci. Rep. 12 (1) (2022) 3507.
[53] J.W. Leem, M.J. Fraser, Y.L. Kim, Transgenic and diet-enhanced silk production for reinforced biomaterials: a metamaterial perspective, Annu Rev. Biomed. Eng. 22 (2020) 79–102.
[54] X. Zhang, L. Xia, B.A. Day, T.I. Harris, P. Oliveira, C. Knittel, A.L. Licon, C. Gong, G. Dion, R.V. Lewis, J.A. Jones, CRISPR/Cas9 initiated transgenic silkworms as a natural spinner of spider silk, Biomacromolecules 20 (6) (2019) 2252–2264.
[55] K. Arakawa, N. Kono, A.D. Malay, A. Tateishi, N. Ifuku, H. Masunaga, R. Sato, K. Tsuchiya, R. Ohtoshi, D. Pedrazzoli, A. Shinohara, Y. Ito, H. Nakamura, A. Tanikawa, Y. Suzuki, T. Ichikawa, S. Fujita, M. Fujiwara, M. Tomita, S. J. Blamires, J.A. Chuah, H. Craig, C.P. Foong, G. Greco, J. Guan, C. Holland, D. L. Kaplan, K. Sudesh, B.B. Mandal, Y. Norma-Rashid, N.A. Oktaviani, R.C. Preda, N. M. Pugno, R. Rajkhowa, X. Wang, K. Yazawa, Z. Zheng, K. Numata, 1000 spider silkomes: linking sequences to silk physical properties, Sci. Adv. 8 (41) (2022) eabo6043.
[56] C. Holland, K. Numata, J. Rnjak-Kovacina, F.P. Seib, The biomedical use of silk: past, present, future, Adv. Health Mater. 8 (1) (2019) e1800465.
[57] S. Hazra, S. Chowdhury, R. Guha, D. Naskar, N. Pradhan, S. Kundu, A. Konar, silk films with natural RGD sequence supports corneal cell proliferation: a promising new biomaterial for corneal regeneration, Invest. Ophthalmol. Vis. Sci. 56 (7) (2015), 3470-3470.
[58] M. Li, W. Tao, S. Lu, C. Zhao, Porous 3-D scaffolds from regenerated Antheraea pernyi silk fibroin, Polym. Advan Technol. 19 (3) (2008) 207–212.
[59] X. Liu, L.X. Shi, X.Z. Wan, B. Dai, Y.P. Chen, S.T. Wang, Recent progress of spider-silk-inspired adhesive materials, Acs Mater. Lett. 3 (10) (2021) 1453–1467.
[60] J. Li, S. Li, J. Huang, A.Q. Khan, B. An, X. Zhou, Z. Liu, M. Zhu, Spider silk-inspired artificial fibers, Adv. Sci. (Weinh.) 9 (5) (2022) e2103965.
[61] A. Leppert, G. Chen, D. Lama, C. Sahin, V. Railaite, O. Shilkova, T. Arndt, E. G. Marklund, D.P. Lane, A. Rising, M. Landreh, Liquid-liquid phase separation primes spider silk proteins for fiber formation via a conditional sticker domain, Nano Lett. 23 (12) (2023) 5836–5841.
[62] B. Schmuck, G. Greco, T.B. Pessatti, S. Sonavane, V. Langwallner, T. Arndt, A. Rising, Strategies for making high-performance artificial spider silk fibers, Adv. Funct. Mater. 34 (35) (2024) 2305040.
[63] T. Arndt, G. Greco, B. Schmuck, J. Bunz, O. Shilkova, J. Francis, N.M. Pugno, K. Jaudzems, A. Barth, J. Johansson, A. Rising, Engineered spider silk proteins for biomimetic spinning of fibers with toughness equal to dragline silks, Adv. Funct. Mater. 32 (23) (2022) 2200986.
[64] J. Chen, A. Tsuchida, A.D. Malay, K. Tsuchiya, H. Masunaga, Y. Tsuji, M. Kuzumoto, K. Urayama, H. Shintaku, K. Numata, Replicating shear-mediated self-assembly of spider silk through microfluidics, Nat. Commun. 15 (1) (2024) 527.
[65] N.N. Ashton, R.J. Stewart, Self-recovering caddisfly silk: energy dissipating, Ca(2+)-dependent, double dynamic network fibers, Soft Matter 11 (9) (2015) 1667–1676.
[66] O. Stefanović, F. Vukajlović, T. Mladenović, D. Predojević, L. Čomić, S.B. Pešić, Antimicrobial activity of Indian meal moth silk, Plodia interpunctella, Curr. Sci. 118 (10) (2020) 1609.
[67] M. Milutinović, D. Čurović, D. Nikodijević, F. Vukajlović, D. Predojević, S. Marković, S. Pešić, The silk of Plodia interpunctella as a potential biomaterial and its cytotoxic effect on cancer cells, Anim. Biotechnol. 31 (3) (2020) 195–202.
[68] A.Y. Kawahara, C.G. Storer, A. Markee, J. Heckenhauer, A. Powell, D. Plotkin, S. Hotaling, T.P. Cleland, R.B. Dikow, T. Dikow, R.B. Kuranishi, R. Messcher, S. U. Pauls, R.J. Stewart, K. Tojo, P.B. Frandsen, Long-read HiFi sequencing correctly assembles repetitive heavy fibroin silk genes in new moth and caddisfly genomes, GigaByte 2022 (2022) gigabyte64.
[69] B.C. Wu, I. Sauman, H.O. Maaroufi, A. Zaloudikova, M. Zurovcova, B. Kludkiewicz, M. Hradilova, M. Zurovec, Characterization of silk genes in Ephestia kuehniella and Galleria mellonella revealed duplication of sericin genes and highly divergent sequences encoding fibroin heavy chains, Front Mol. Biosci. 9 (2022) 1023381.
[70] D. Silhacek, G. Miller, Growth and development of the Indian meal moth, Plodia interpunctella (Lepidoptera: Phycitidae), under laboratory mass-rearing conditions, Ann. Èntomol. Soc. Am. 65 (5) (1972) 1084–1087.
[71] O. Foster, S. Shaidani, S.K. Theodossiou, T. Falcucci, D. Hiscox, B.M. Smiley, C. Romano, D.L. Kaplan, Sudan Black B pretreatment to suppress autofluorescence in silk fibroin scaffolds, ACS Biomater. Sci. Eng. 9 (6) (2023) 3193–3205.
[72] P.Y. Neo, D.J. Tan, P. Shi, S.L. Toh, J.C. Goh, Enhancing analysis of cells and proteins by fluorescence imaging on silk-based biomaterials: modulating the autofluorescence of silk, Tissue Eng. Part C. Methods 21 (2) (2015) 218–228.
[73] H. Sehadova, R. Zavodska, L. Rouhova, M. Zurovec, I. Sauman, The role of Filippi's glands in the silk moths cocoon construction, Int J. Mol. Sci. 22 (24) (2021).
[74] S. Patra, R.N. Singh, M. Raziuddin, Morphology and histology of Lyonet's gland of the tropical tasar silkworm, Antheraea mylitta, J. Insect Sci. 12 (2012) 123.
[75] X. Wang, Y. Li, Q. Liu, X. Tan, X. Xie, Q. Xia, P. Zhao, GC/MS-based metabolomics analysis reveals active fatty acids biosynthesis in the Filippi's gland of the silkworm, Bombyx mori, during silk spinning, Insect Biochem Mol. Biol. 105 (2019) 1–9.
[76] R. Fedic, M. Zurovec, F. Sehnal, Correlation between fibroin amino acid sequence and physical silk properties, J. Biol. Chem. 278 (37) (2003) 35255–35264.
[77] A. Gaviria, N. Jaramillo-Quiceno, A. Motta, A. Restrepo-Osorio, Silk wastes and autoclaved degumming as an alternative for a sustainable silk process, Sci. Rep. 13 (1) (2023) 15296.
[78] A.K. Childers, S.M. Geib, S.B. Sim, M.F. Poelchau, B.S. Coates, T.J. Simmonds, E. D. Scully, T.P.L. Smith, C.P. Childers, R.L. Corpuz, K. Hackett, B. Scheffler, The USDA-ARS Ag100Pest initiative: high-quality genome assemblies for agricultural pest arthropod research, Insects 12 (7) (2021) 626.
[79] J.O. Warwicker, Comparative studies of fibroins. II. The crystal structures of various fibroins, J. Mol. Biol. 2 (6) (1960) 350–362.
[80] W.L. Stoppel, N. Raia, E. Kimmerling, S. Wang, C.E. Ghezzi, D.L. Kaplan, 2.12 Silk Biomaterials, in: P. Ducheyne (Ed.), Comprehensive Biomaterials II, Elsevier, Oxford, 2017, pp. 253–278.
[81] H.Y. Wang, Y.Q. Zhang, Z.G. Wei, Characterization of undegraded and degraded silk fibroin and its significant impact on the properties of the resulting silk biomaterials, Int J. Biol. Macromol. 176 (2021) 578–588.
[82] C. Holland, N. Hawkins, M. Frydrych, P. Laity, D. Porter, F. Vollrath, Differential scanning calorimetry of native silk feedstock, Macromol. Biosci. 19 (3) (2019) e1800228.
[83] M. McGill, G.P. Holland, D.L. Kaplan, Experimental methods for characterizing the secondary structure and thermal properties of silk proteins, Macromol. Rapid Commun. 40 (1) (2019) e1800390.
[84] G.B. Perea, C. Solanas, N. Marí-Buyé, R. Madurga, F. Agulló-Rueda, A. Muinelo, C. Riekel, M. Burghammer, I. Jorge, J. Vázquez, The apparent variability of silkworm (Bombyx mori) silk and its relationship with degumming, Eur. Polym. J. 78 (2016) 129–140.
[85] J. Liu, L. Shi, Y. Deng, M. Zou, B. Cai, Y. Song, Z. Wang, L. Wang, Silk sericin-based materials for biomedical applications, Biomaterials 287 (2022) 121638.
[86] G. Greco, B. Schmuck, S.K. Jalali, N.M. Pugno, A. Rising, Influence of experimental methods on the mechanical properties of silk fibers: a systematic literature review and future road map, Biophys. Rev. (Melville) 4 (3) (2023) 031301.

[87] K. Min, J.D. Cuiffi, R.T. Mathers, Ranking environmental degradation trends of plastic marine debris based on physical properties and molecular structure, Nat. Commun. 11 (1) (2020) 727.
[88] E. Malikmammadov, T.E. Tanir, A. Kiziltay, V. Hasirci, N. Hasirci, PCL and PCL-based materials in biomedical applications, J. Biomater. Sci. Polym. Ed. 29 (7-9) (2018) 863–893.
[89] C. Choong, J.T. Triffitt, Z.F. Cui, Polycaprolactone scaffolds for bone tissue engineering - Effects of a calcium phosphate coating layer on osteogenic cells, Food Bioprod. Process 82 (C2) (2004) 117–125.
[90] D. Mondal, M. Griffith, S.S. Venkatraman, Polycaprolactone-based biomaterials for tissue engineering and drug delivery: current scenario and challenges, Int. J. Polym. Mater. Polym. Biomater. 65 (5) (2016) 255–265.
[91] S.R. Shah, C.D. Modi, S. Singh, D.D. Mori, M.M. Soniwala, B.G. Prajapati, Recent advances in additive manufacturing of polycaprolactone-based scaffolds for tissue engineering applications: a comprehensive review, Regen. Eng. Transl. Med. (2024) 1–20.
[92] L.J. Gibson, M.F. Ashby, B.A. Harley, Cellular Materials in Nature and Medicine, Cambridge University Press, 2010.
[93] D.T. Govindaraju, C.H. Chen, K.T. Shalumon, H.H. Kao, J.P. Chen, Bioactive nanostructured scaffold-based approach for tendon and ligament tissue engineering, Nanomaterials (Basel) 13 (12) (2023) 1847.
[94] A. Motta, C. Migliaresi, A.W. Lloyd, S.P. Denyer, M. Santin, Serum protein absorption on silk fibroin fibers and films: surface opsonization and binding strength, J. Bioact. Compat. Pol. 17 (1) (2002) 23–35.
[95] Y. Wang, D.D. Rudym, A. Walsh, L. Abrahamsen, H.J. Kim, H.S. Kim, C. Kirker-Head, D.L. Kaplan, In vivo degradation of three-dimensional silk fibroin scaffolds, Biomaterials 29 (24-25) (2008) 3415–3428.
[96] A.E. Thurber, F.G. Omenetto, D.L. Kaplan, In vivo bioresponses to silk proteins, Biomaterials 71 (2015) 145–157.
[97] W.L. Stoppel, A.E. Gao, A.M. Greaney, B.P. Partlow, R.C. Bretherton, D.L. Kaplan, L.D. Black, 3rd, Elastic, silk-cardiac extracellular matrix hydrogels exhibit time-dependent stiffening that modulates cardiac fibroblast response, J. Biomed. Mater. Res. A 104 (12) (2016) 3058–3072.
[98] W.L. Stoppel, D. Hu, I.J. Domian, D.L. Kaplan, L.D. Black, 3rd, Anisotropic silk biomaterials containing cardiac extracellular matrix for cardiac tissue engineering, Biomed. Mater. (Bristol Engl.) 10 (3) (2015) 034105.
[99] C.E. Ghezzi, L. Wang, I. Behlau, J. Rnjak-Kovacina, S. Wang, M.H. Goldstein, J. Liu, J.K. Marchant, M.I. Rosenblatt, D.L. Kaplan, Degradation of silk films in multipocket corneal stromal rabbit models, J. Appl. Biomater. Func. 14 (3) (2016) e266–e276.